Universidade de Aveiro Departamento de Física,
2020

**João Pedro
Dias Rodrigues**

A study of possible beyond the standard model frameworks containing multiple scalars and their implications in the search for new physics.

Um estudo de modelos numa arquitetura para além do modelo padrão e o seu possível impacto em nova física

o júri / the jury

presidente

Margarida Facão
Professora Auxiliar do Departamento de Física da Universidade de Aveiro

vogais

António Morais
Investigador Nível 1 do Departamento de Física da Universidade de Aveiro

Nuno Castro
Professor Assistente da University of Minho.

agradecimentos / acknowledgements

Honestamente acho que isto vai ter que ser escrito antes da entrega,REMINDER agradecer ao Morais! Pedro Ferreira Roman e Ian, sem o trabalho deles estava perdido.

Honestly this will be written in english translated poorly from above :)

Resumo

O Modelo Padrão é neste momento o paradigma na analise de física de particulas, este une numa arquitectura autoconsistente e propriamente motivada três das quatro forças fundamentais do universo, no entanto, o consenso cientifico é que modelo padrão esta incompleto, visto que apesar do excelente acordo entre muitas das suas previsões e a realidade, imensas experiencias estão a mostrar fenómenos que o modelo padrão não consegue reconsiliar.

Devido a estas falhas, estão cada vez mais a ser propostos modelos motivados por objectivos, como a inclusão de grande unificação ou a previsão de materia escura, para tentar completar ou substituir o modelo padrão.

Neste trabalho começamos por uma breve revisão do Modelo Padrão, e de seguida apresentamos dois modelos que se intintulam para alem do modelo padrão com o objectivo de os introduzir toericamente como contexto para a apresentação de uma analise numerica sobre os possíveis sinais de nova física que cada senario podera trazer.

Abstract This part will be in English. Translated from above.

Contents

List of Figures

List of Tables

Chapter 1

Introduction

Our current understanding of all subatomic phenomena must be understood trough the Standard Model (SM) of particle physics. The SM has thus far been the best descriptor for the experimentally observed spectra of particles and their interactions at the electroweak (EW) scale. In 2012 a resonance was discovered at the Large Hadron Collider (LHC) that seems to confirm the existence of its last predicted particle, the Higgs boson, finally completing the Model and proving the existence of the Higgs mechanism [1, 2, 3, 4].

The development of the SM was a arduous task, it led scientists successfully combine three of the four fundamental forces of nature in a well motivated framework, making it one of the most monumental achievements in theoretical physics. However, despite its successes the SM still lacks a strong explanation for several experimental observations.

First, we have the fact that the SM can not account for one of the most important cosmological discoveries of the century, the existence of dark matter [5]. This is a fundamental flaw since the SM lacks a possible dark matter candidate, or dark particle (Do I need a citation for this claim?). Secondly, neither the SM, nor the theory of general relativity, offer any justification for the existence of baryon asymmetry in the universe, i.e. why is the universe primarily made of matter rather than anti-matter [6]. Note, that a popular proposed scenario as to explain cosmic baryon asymmetry is the Electroweak baryogenesis (EWBG) which requires some sort of new physics (NP) structure [7]. Thirdly, the SM suffers from peculiar oddities in the fermion sector in the form of unjustified mass and mixing hierarchies. This is usually refereed to as the flavour problem and is considered a sizeable drawback of the SM. As an example, we observe the top quark mass ($\mathcal{O}(100)$ GeV) to be five order of magnitudes heavier than the up quark ($\mathcal{O}(1)$ MeV), and eleven orders of magnitude above the observed neutrino masses ($\mathcal{O}(1)$ eV). These high differences are thought to be too large to be natural, so a physical property that would justify such gap is a desired property of most Beyond the Standard Model (BSM) frameworks. Fourth, neutrino masses are not included in the SM. Although there are precise oscillation measurements that measure masses differences in the eV range with precise mixing in between 3 different generations of neutrinos [8]. There are still many other subtitle flaws, like the lack of a strong phase transition, the R_κ parameter and $g-2$ anomaly of lepton magnetic moments, etc.

These are just some of the typical justifications given to explore possible BSM scenarios. The holy grail of which would be a model that solves all these problems in a properly motivated framework that addresses these and many more cosmological and phenomenological problems. For now such a model remains far out of reach, so the narrowing down of theories through phenomenological studies is a very worthwhile endeavour. We try to present one of these studies in this work. The goal of performing these types of analysis is to narrow down it's renaming parameter space and see how much phenomenology it can explain, or not, and even perhaps exclude the model under modern collider experiments. Paradoxically, as of late these studies have become progressively harder to perform given that the available space for NP gets reduced by each successful particle experiment. Chief among them are the ATLAS, CMS experiments and the LHC, whose large amount of collect data over past years is setting ever more stringent bounds on viable parameter spaces of popular BSM scenarios. And as available space for new physics decreases it becomes more challenging to reveal remaining space without falling within the possibility of fine tuning our model.

Note, that the SM has shown itself consistence with most constraints that were initial believed to be a possible gateway to NP i.e. diverge from its predictions. Thus, the search continues for hints at possible directions to complete the SM. Conventionally, phenomenological simulations of BSM searches in these multi-dimensional parameter spaces have been made in large computer-clusters requiring several weeks of computational time trough simple Monte-Carlo methods. This is the basis for the work presented here although some modern studies have incorporated new methods to scan these complex problems like machine learning.

During this thesis we embark in a small expedition into two possible BSM scenarios. To achieve this, we will start by laying down the fundamental basis for this BSM discussion by presenting a short overview of the SM followed by a discussion into potential extensions of this framework. First by presenting the B-L-SM model. Then, we move on to a more complex model with additional Higgs doublets fields as a an attempt to present a framework that addresses the flavour problem. We will see how each of these models addresses problems differently and discuss the advantages and disadvantages of a simple unitarity extension versus a multiple doublet approach and vice-versa. For example multiple Higgs doubles can easily offer an explanation for the observed excess of charge parity or $\mathcal{CP}$ violation but suffer from the possible inclusion of tree-level Flavour Changing Neutral Currents (FCNCs). These FCNCs are undesirable [9], at least in large number given current observations, so mechanisms have to be put in place to prevent them, while in the case of the simple unitary extensions such problems tend to not arise [10].

I also want to stress that, while the minimal structure of the Higgs sector postulated by the SM is not an immediate contradiction to experimental measurements. It is not manifestly required by the data. In fact an extended scalar sector is often desirable despite the tight bounds on Higgs boson couplings to SM gauge boson and heavy fermions. citation?. These additions are partially motivated by the fact that in the SM, the single Higgs doublet is a bit "overstretched". It takes care simultaneously, of the gauge boson masses, up and down-type quarks masses and leptons masses. N-Higgs-doublet models have multiple scalar and complex fields that can relax this, while the unitary additions cannot address this observation citation?. In fact these multiple Higgs doublet models are often engineered based on a naturalness argument, that is, that the notion of generations can be brought to the Higgs sector and these might help explain mass hierarchies. This isn't the particular case of the model we will present in this thesis.

Chapter 2

The Standard Model of Particle Physics

As stated in chapter 1, it is hard to question the validity of the SM as a successful, at least approximate, framework with whom to describe the phenomenology of particle physics up to the largest energy scales probed by collider measurements so far although some inconsistencies remain and must be addressed.

What we call the SM is the conjugation of several theories, quantum chromodynamics (QCD), Higgs sector and electroweak (EW) theory. The last piece, the EW theory was introduced in the nineteen sixties by Glashow, Salam and Weinberg [11] and since it has been extensively tested both in contemporary direct searches for new physics and indirect probes via e.g. flavour anomalies and precise electroweak parameter measurements in proton-electron collisions [12]. It awarded the authors the 1979 Noble prize of physics [13].

The path to the formulation of the SM came from previous principles relating to symmetries in nature, specifically symmetry in physical laws. In fact, much in modern physics can be attributed to Emmy Noether's work. She deduced, trough her first theorem, that if the action in a system is invariant under some group of transformations (symmetry), then there exist one or more conserved quantities (constants of motion) [14].

Physicists took this idea and were led to the fundamental question behind the SM, is it possible that upon imposing to a given Lagrangian the invariance under a certain group of symmetries to reach a given form for its the dynamics? We can quote Salam and Ward in Ref [12]:

"Our basic postulate is that it should be possible to generate strong, weak and electromagnetic interaction terms (with all their correct symmetry properties and also with clues regarding their relative strengths) by making local gauge transformations on the kinetic energy terms in the free Lagrangian for all particles."

We are glossing over a lot of complexity here, and for the SM to be properly formulated, additional concepts are required. In the case of the weak interactions, the presence of a massive weak gauge boson requires the concept of spontaneous breakdown of the gauge symmetry via what is known as the Higgs mechanism [15, 16, 17]. While the concept of asymptotic freedom played a crucial role in describing perturbatively the strong interaction at short distances [18, 19].

2.1 Internal symmetry of the Standard Model

The SM is a gauge Quantum Field Theory (QFT) theory, that is, it is manifestly invariant under a set of field transformations. The SM gauge group [20], $\mathcal{G}_{SM}$, is seen in,

$$\mathcal{G}_{SM} = \mathrm{SU}(3)_{\mathrm{c}} \times \mathrm{SU}(2)_{\mathrm{L}} \times \mathrm{U}(1)_{\mathrm{Y}} \quad . \tag{2.1}$$

Where, $\mathrm{SU}(3)_{\mathrm{C}}$, with C being colour, is the group that describes the QCD sector, responsible for the strong force. This symmetry will remain unbroken by the electroweak vacuum expectation value (VEV). Secondly, we have the $\mathrm{SU}(2)_\mathrm{L} \times \mathrm{U}(1)_\mathrm{Y}$ portion, with L being Left and Y the hypercharge, that will be broken by the Higgs mechanism into $\mathrm{U}(1)_\mathrm{Q}$, the electromagnetic gauge symmetry. Each particle stems from a field that is charged in a particular manner on each of these groups. Given the invariance under the group in Eq. (2.1), it is impossible for any field, besides the scalar field, to have an explicit mass term in the bare Lagrangian. This chapter will focus on how the mass of particles is generate via the Higgs mechanism. And offer a brief discussion of flavour physics in the SM and how flavour changing currents can point to NP.

Gauge Group numbers

The full set of quantum numbers for the SM fields are are shown in the tables 2.1 and 2.2. These show us the representations of these fields, e.g. if a field F has a quantum number of 3 under $\mathrm{SU}(2)_\mathrm{L}$ then he would be a triplet of of $\mathrm{SU}(2)_\mathrm{L}$, $F^a = (F^1, F^2, F^3)$, where a is the adjoint representation of the group.

Table 2.1: Gauge and Scalar fields in the SM

Fields	Spin 0 field	Spin 1 Field	$SU(3)_C \times SU(2)_L \times U(1)_Y$
Gluons	$\times$	G^a	$(\mathbf{8},\mathbf{1},0)$
A bosons	$\times$	A^a	$(\mathbf{1},\mathbf{3},0)$
B bosons	$\times$	B	$(\mathbf{1},\mathbf{1},0)$
Higgs field	$(\phi^\pm, \phi^0)$	$\times$	$(\mathbf{1},\mathbf{2},1)$

Table 2.2: Fermion fields in the SM

Fields	Spin $\frac{1}{2}$ Field	$SU(3)_C \times SU(2)_L \times U(1)_Y$
Quarks (3 gen.)	$Q = (u_L, d_L)$	$(\mathbf{3}, \mathbf{2}, 1/3)$
	u_R	$(\mathbf{3}, \mathbf{1}, 4/3)$
	d_R	$(\mathbf{3}, \mathbf{1}, -2/3)$
Leptons (3 gen.)	$(L = (\nu_{e_L}, e_L)$	$(\mathbf{1}, \mathbf{2}, -1)$
	e_R	$(\mathbf{1}, \mathbf{1}, -2)$

From here, given the gauge group in, Eq. (2.1) and accounting for the charges and fields, we can derive the form of the SM's Lagrangian. These gauge groups are composed of 12 generators and are governed by the following algebra,

$$[M_a, M_b] = i f_{abc} M_c \quad [T_a, T_b] = 1\epsilon_{abc} T_c \quad [M_a, T_b] = [M_a, Y] = [T_b, Y] = 0 \tag{2.2}$$

where for $\mathrm{SU}(3)_\mathrm{c}$, $M_a = \lambda_a/2$, with $(a = 1, ..., 8)$. As for $\mathrm{SU}(2)_\mathrm{L}$, we have $T_i = \frac{\sigma_i}{2}$, $(i = 1, 2, 3)$, and for Y is the generator of $U(1)_Y$. The symbols λ_a and σ_i represent the Gell-Mann and Pauli matrices respectively.

2.1.1 Fields, Particles and Lagrangian of the SM

From these fields, the particle spectrum of the SM is composed by, the gauge bosons, $W^\pm$ and Z bosons mediators of the weak interactions, the photon γ, the electromagnetic interaction messenger and the strong force mediators, the gluons, G, as well as by the matter particles, the fermions, composed by the quarks and leptons. A spin-0 scalar also emerges known as the Higgs Boson, h.

Leptons and quarks are organized in three generations each, with 2 pairs by each generation leading to 6 different particles. For quarks we have the up and down for the first generation, charm and strange for the second as well as the top and bottom for the third one. Similarly, there are 6 types of leptons, the charged ones, electron, muon and tau, and the associated neutrinos. These are represented in different manners, being that the quarks are represented by the letters (u, d, c, s, t, b) while leptons as $(e, \nu_e, \mu, \nu_\mu, \tau, \nu_\tau)$.

Fermions are half integer spin particles half of which have electrical charge (except the neutrinos). While quarks interact via the weak, electromagnetic and strong forces, the charged leptons only feel the electromagnetic and weak forces and the neutrinos are weakly interacting. A physical fermion is composed of a left-handed and a right-handed field. The left-handed components of the fermions are doublets under $\mathrm{SU}(2)_L$,

$$L^i = \begin{pmatrix} \nu_{e_L} \\ e_L \end{pmatrix}, \begin{pmatrix} \nu_{\mu_L} \\ \mu_L \end{pmatrix}, \begin{pmatrix} \nu_{\tau_L} \\ \tau_L \end{pmatrix} \quad \text{and} \quad Q^i = \begin{pmatrix} u_L \\ d_L \end{pmatrix}, \begin{pmatrix} c_L \\ s_L \end{pmatrix}, \begin{pmatrix} t_L \\ b_L \end{pmatrix} \quad , \tag{2.3}$$

where the i index stands for generation, often designed as the flavour index. Conversely the right-handed components are singlets of $\mathrm{SU(2)_L}$ and are represented as,

$$e^i_R = \{e_R, \mu_R, \tau_R\}, \quad u^i_R = \{u_R, c_R, t_R\}, \quad d^i_R = \{d_R, s_R, b_R\} \quad , \tag{2.4}$$

note also that the quarks form triplets of $\mathrm{SU(3)_C}$ whereas leptons are colour singlets, meaning that only quarks interact strongly. The Higgs boson also emerges from an $\mathrm{SU(2)_L}$ doublet with the form,

$$H = \begin{pmatrix} \phi^1 + i\,\phi^2 \\ \phi^3 + i\,\phi^4 \end{pmatrix}, \tag{2.5}$$

where we see the four components that correspond to the respective degrees of freedom of the Higgs Field. After the process of SSB of the $\mathrm{SU(2)_L} \times \mathrm{U(1)_Y}$ group the charges,

Table 2.3: Quark and Lepton charges

	$\mathrm{SU(3)_C}$	$\mathrm{U(1)_Q}$
Up type quarks (u, c, t)	**3**	2/3
Down type quarks (d, s, b)	**3**	-1/3
Charged leptons (e, μ, τ)	**1**	-1
Neutrinos $(\nu_e, \nu_\mu, \nu_\tau)$	**1**	0

Lagrangian formulation

Given the SM gauge groups seen in Eq. (2.1) and charges seen in Tables 2.1 and 2.2 the covariant derivative, D_μ, reads as,

$$D_\mu = \partial_\mu - i g_s M^a G^a_\mu - i g T^i A^i_\mu - \frac{1}{2} i g' Y B_\mu \quad , \tag{2.6}$$

We can expect 3 different type of couplings, g_s related to the $\mathrm{SU(3)_C}$ subgroup, g to the $\mathrm{SU(2)_L}$ and g' to $\mathrm{U(1)_Y}$. The associated canonical field strength tensors would be,

$$G^{\mu\nu}_a = \partial^\mu G^\nu_a - \partial G^\mu_a - g_s f_{abc} G^\mu_a G^\nu_b \tag{2.7}$$

$$A^{\mu\nu}_a = \partial^\mu A^\nu_a - \partial^\nu A^\mu_a - g \epsilon_{abc} A^\mu_b A^\nu_c \tag{2.8}$$

$$B^{\mu\nu} = \partial^\mu B^\nu - \partial^\nu B^\mu \tag{2.9}$$

It is often convenient to present the SMs Lagrangian in portions, usually divided in three [1] sections,

$$\mathcal{L}_{SM} = \mathcal{L}_{kin} + \mathcal{L}_{Yuk} + \mathcal{L}_\phi \tag{2.10}$$

[1]Of course, there is also the need for the introduction of gauge fixing terms and ghosts. However, this is merely a formal requirement and does not imply addition of new physical states.

Where we have the kinetic portion of the SM terms,$\mathcal{L}_{kin}$, responsible for free propagation of particles, the Yukawa portion, $\mathcal{L}_{Yuk}$ corresponding to interactions of particles with the Higgs Boson, and finally the $\mathcal{L}_{\phi}$ scalar potential. The full kinetic portion of the SM read,

$$\begin{aligned}\mathcal{L}_{kin} = &-\frac{1}{4}G_a^{\mu\nu}G_{a\,\mu\nu} - \frac{1}{4}A_a^{\mu\nu}A_{a\,\mu\nu} - \frac{1}{4}B^{\mu\nu}B_{\mu\nu} \\ &- i\bar{Q}_{L_i}\not{D}Q_{L_i} - i\bar{u}_{R_i}\not{D}u_{R_i} - i\bar{d}_{R_i}\not{D}d_{R_i} - i\bar{L}_{L_i}\not{D}L_{L_i} - i\bar{e}_{R_i}\not{D}e_{R_i} \\ &- (D_\mu H)^\dagger(D^\mu H),\end{aligned} \tag{2.11}$$

where $\not{D}$ is the Dirac covariant derivative, $\gamma^\mu D_\mu$. From the last line of Eq. (2.11) and with Eq. (2.6) we will present how the fields A_μ^a and B_μ give rise to the weakly interacting vector bosons $W^\pm$ and Z^0 and the electromagnetic vector boson γ. Contrary to the colour sector, where the eight generators G_μ^a simply correspond to eight gluons G mediating the strong interactions. The scalar potential part is written as,

$$\mathcal{L}_\phi = -\mu^2 HH^\dagger - \lambda(HH^\dagger)^2. \tag{2.12}$$

Finally the Yukawa portion of the Lagrangian is,

$$\mathcal{L}_{Yuk} = Y_{ij}^u\overline{Q_{L_i}}u_{R_j}\tilde{H} + Y_{ij}^d\overline{Q_{L_i}}d_{R_j}H + Y_i^e j\overline{L_{L_i}}e_{R_i}H + \text{H.c.}, \tag{2.13}$$

where, $\tilde{H} = i\sigma_2 H$ and H.c. stands for Hermitian conjugate, also the terms $Y^{e,u,d}$ stands for the Yukawa matrices, these are generic 3×3 with complex and non-dimensional matrix elements. Note that all indices seen in Eqs. (2.11), (2.12) and (2.13), (j,i) are summed over.

2.2 The Higgs mechanism and the mass generation of the Gauge bosons

From what was defined above, we can now study the process SSB by which,

$$\mathrm{SU(2)_L \times U(1)_Y \to U(1)_Q}. \tag{2.14}$$

Enabling us to find the real physical states of the gauge bosons and the origin of their mass. Let us consider the part of the Lagrangian containing the scalar covariant derivatives, the scalar potential and the gauge-kinetic terms:

$$\mathcal{L}_{Gauge} \supset (D_\mu H)(D^\mu H)^\dagger - \mu^2 H^\dagger H - \lambda(H^\dagger H)^2 - \frac{1}{4}W_a^{\mu\nu}W_{a\,\mu\nu} - \frac{1}{4}B^{\mu\nu}B_{\mu\nu}. \tag{2.15}$$

We expect a phase shift to occur, namely one that ensures $\mu^2 < 0$ while at the same ensuring that the field now explicitly breaks the $\mathrm{SU(2)_L \times U(1)_Y}$. For this to happen we expect the shifted squared value of the Higgs field to be,

$$(H^\dagger H)^2 = \frac{-\mu^2}{2\lambda} \equiv v^2, \tag{2.16}$$

called the electroweak VEV, is experimentally measured to be $v \approx 246$ GeV. The choice of vacuum can be aligned in such a way that we have,

$$H_{min} = \frac{1}{\sqrt{2}}\begin{pmatrix}0\\ v\end{pmatrix}. \tag{2.17}$$

Given that now the $SU(2)_L \times U(1)_Y$ symmetry is broken down to $U(1)_Q$ we jump from a scenario where there were four generators, which are $T^{1,2,3}$ and Y, to, after the breaking, having solely one unbroken combination that is $Q = (T^3 + 1/2)$ associated to the electric charge. This means that in total we will have three broken generators, thus, from the Goldstone theorem, there would have to be created three massless particles.

These Goldstones modes however can be parameterized as phases in field space and can be "rotated away" in the physical basis, leaving us with a single physical massive scalar, the Higgs boson. Note that, with this transformation we are removing three scalar degrees of freedom. However, they cannot just disappear from the theory and will be absorbed by the massive gauge bosons. In fact, a massless gauge boson contains only two scalar degrees of freedom (transverse and polarization). Meanwhile, a massive vector boson has two transverse and a longitudinal polarization, i.e., three scalar degrees of freedom. So, as we discussed above, while before the breaking of the EW symmetry we have four massless gauge bosons, after the breaking we are left with three massive ones. This means that there are three extra scalar degrees of freedom showing up in the gauge sector. It is then commonly said that the goldstone bosons are "eaten" by the massive gauge bosons and the total number of scalar degrees of freedom in the theory is preserved. Therefore, without loss of generality, we can rewrite the Higgs doublet as

$$\begin{pmatrix} G_1 + iG_2 \\ v + h + iG_3 \end{pmatrix} = H \to H = \frac{1}{\sqrt{2}} \begin{pmatrix} 0 \\ v + h \end{pmatrix}. \tag{2.18}$$

Once the Higgs doublet acquires a VEV, the Lagrangian (2.15) can be recast as:

$$\begin{aligned} \mathcal{L}' =& \frac{1}{2}\partial_\mu h \partial^\mu h - \frac{1}{2}(2v^2\lambda)h^2 - \frac{1}{4}W_a^{\mu\nu}W_{a\,\mu\nu} - \frac{1}{4}B^{\mu\nu}B_{\mu\nu} \\ &+ \frac{1}{8}v^2 g^2 (A_\mu^1 A^{1,\mu} + A_\mu^2 A^{2,\mu}) + \frac{1}{8}v^2(g^2 A_\mu^3 A^{3,\mu} + g'^2 B_\mu B^\mu - 2g^2 g'^2 A_\mu^3 B^\mu), \end{aligned} \tag{2.19}$$

A few things become obvious. First, we have a lot of mass terms stemming from the squared gauge fields and a lonesome mass term belonging to the real scalar field we know to be the Higgs field. This makes the Higgs boson mass to be given by,

$$M_h = (2v^2\lambda). \tag{2.20}$$

To obtain masses for the gauge bosons we need to rotate the gauge fields to a basis where the mass terms are diagonal. First, it is straightforward to see that the electrically charged eigenstates are given by

$$W_\mu^\pm = \frac{1}{\sqrt{2}}(A_\mu^{(1)} \pm iA_\mu^{(2)}), \tag{2.21}$$

meaning that the mass of the W bosons is,

$$M_{W^\pm} = \frac{1}{2}vg. \tag{2.22}$$

The situation becomes a bit more complicated for the second term in (2.19) due to a mixing between A_μ^3 and B_μ. In the gauge eigenbasis the mass terms read

$$\begin{pmatrix} A_\mu^3 & B_\mu \end{pmatrix} \cdot \frac{1}{4}\nu^2 \begin{pmatrix} g^2 & -gg' \\ -gg' & g'^2 \end{pmatrix} \cdot \begin{pmatrix} A_\mu^3 \\ B_\mu \end{pmatrix}, \tag{2.23}$$

which can be diagonalized to obtain,

$$\begin{pmatrix} A_\mu & Z_\mu \end{pmatrix} \begin{pmatrix} 0 & 0 \\ 0 & \frac{1}{2}v\sqrt{g^2 + g'^2} \end{pmatrix} \begin{pmatrix} A^\mu \\ Z^\mu \end{pmatrix}, \tag{2.24}$$

we identify the eigenvector associated with the null eigenvalue to be the photon and the massive one, $M_Z = \frac{1}{2}v\sqrt{g^2 + g'^2}$, to be the Z boson. Such eigenvectors can be written as

$$A_\mu = \cos(\theta_W)B_\mu + \sin(\theta_W)A_\mu^3, \tag{2.25}$$

$$Z_\mu = -\sin(\theta_W)B_\mu + \cos(\theta_W)A_\mu^3, \tag{2.26}$$

where θ_W is the so called Weinberg mixing angle and is defined as,

$$\cos(\theta_W) = \frac{g}{\sqrt{g^2 + g'^2}}. \tag{2.27}$$

Thus showing the massless photon along with a massive Z boson with mass $M_Z = \frac{1}{2}\nu\sqrt{g^2 + g'^2}$. So we conclude our exploration of the electroweak sector with all the correct massive spectrum observed and its origin discussed.

2.3 Fermion Masses in the SM and Quark mixing

As referenced previously, given the charges of the fermion and lepton fields we cannot construct a gauge invariant theory with explicit mass terms for fermions. The mass of these particles are generated through the Higgs mechanism, via Yukawa terms between the fermions and the scalar field. These interactions can be seen in Eq (2.28),

$$\mathcal{L}_{Yuk} = Y^u_{ij}\overline{Q_{L_i}}u_{R_j}\tilde{H} + Y^d_{ij}\overline{Q_{L_i}}d_{R_j}H + Y^e_i j\overline{L_{L_i}}e_{R_i}H + H.c. \tag{2.28}$$

as the Higgs field settles into the electroweak VEV (see Eq. (2.18)) mass terms for the quarks and leptons are generated. The Higgs mechanism generates the mass for all the fermionic and leptonic particles except for neutrinos, this is due to the SM not containing right handed neutrinos, i.e we can not build terms that would lead to neutrino masses. The addition of right handed neutrino fields is very commonly made in BSM scenarios.

To reach the physical states from the weak eigenbasis you must diagonalize the Yukawa matrices. This is done through bi-unitary transformations. We can write these transformation under the form,

$$M^{u,d,e}_{\text{diag.}} = U^{u,d}_L Y^{u,d} U^{u,d}_R \frac{v}{\sqrt{2}}, \tag{2.29}$$

where $U^{u,d}_L$ and $U^{u,d}_R$ are the required 4 unitary matrices.

For simplicities sake we assume that the leptonic Yukawa couplings matrix Y^e is flavour diagonal i.e. a diagonal matrix needing not to be transformed. This makes only the quarks to be relevant to our discussions.

Naturally, we can invert Eq. 2.29, returning,

$$\begin{aligned} Y^u_{ij} =& \frac{\sqrt{2}}{v}(U^u_L M^u_{\text{diag.}} U^u_R)_{ij} \\ Y^d_{ij} =& \frac{\sqrt{2}}{v}(U^d_L M^d_{\text{diag.}} U^d_R)_{ij} \end{aligned} \tag{2.30}$$

Considering the Higgs mechanism, we can see this change creates mass terms for physical quark fields by replacing the result of eq. 2.30 in the Yukawa portion of the Lagrangian (Eq. 2.13).

$$\begin{gathered} \mathcal{L}_{Yuk} \supset -\frac{v}{\sqrt{2}}Y^d_{ij}\begin{pmatrix}\overline{u}_{L\,i} & \overline{d}_{L\,i}\end{pmatrix} d_{R\,j}\tilde{H} - \frac{v}{\sqrt{2}}Y^u_{ij}\begin{pmatrix}\overline{u}_{L\,i} & \overline{d}_{L\,i}\end{pmatrix} u_{R\,j} + H.c. \\ \Downarrow \\ -(U^d_L m^d_{\text{diag.}} U^d_R)_{ij} d_{L\,i}\, d_{R\,j} - (U^u_L m^u_{\text{diag.}} U^u_R)_{ij} u_{L\,i}\, u_{R\,j} + (\text{Interactions with } h) + H.c \\ \Downarrow \\ -m^d_{\text{diag.}_j} d'_{L\,i}\, d'_{R\,j} - m^u_{\text{diag.}_j} u'_{L\,i}\, u'_{R\,j} + (\text{Interactions with h}) + H.c \end{gathered} \tag{2.31}$$

where the primed fields are the quark fields in the mass basis, defined as,

$$\begin{aligned} d'_{L,R} &= U^d_{L,R} d_{L,R} \\ u'_{L,R} &= U^u_{L,R} u_{L,R} \end{aligned} \tag{2.32}$$

Note that the increasing masses seen in each generation depend directly on the hierarchy of the Yukawa terms. This means that the mass of all particles directly relates to how strongly they each interact with the Higgs boson. If you then take into account the real masses e.g. for the leptons, the tau mass is in the GeV range while the electron's is in the 0.1 MeV range. This translate to very different couplings for each flavour. This hierarchy is unjustified in the SM.

As a result of this redefinition we can now look at the gauge interactions to see that charged currents appear where $W^{\pm}$ couples to the physical u'_{L_j} and d'_{L_j} quarks. The coupling of the fermions to the gauge fields changes by virtue of the fact that only left handed quarks are $SU(2)_L$ doublets. If we expand the up and down quark fields on the kinetic portion of the Lagrangian,

$$\begin{aligned}\mathcal{L}_{ferm} \supset & \frac{1}{2}\bar{u}'_L\gamma^{\mu}\left(g'YB_{\mu}+gZ_{\mu}\right)\left(U^u_L U^{u\dagger}_L\right)u'_L - \frac{1}{\sqrt{2}}g\bar{u}'_L\gamma^{\mu}\left(U^u_L U^{d\dagger}_L\right)d'_L W^+_{\mu} \\ & -\frac{1}{\sqrt{2}}g\bar{d}'_L\gamma^{\mu}\left(U^u_L U^{d\dagger}_L\right)u'_L W^-_{\mu} + \frac{1}{2}\bar{d}'_L\gamma^{\mu}\left(g'YB_{\mu}-gZ_{\mu}\right)\left(U^d_L U^{d\dagger}_L\right)d'_L\end{aligned}$$

By employing properties of unitary matrices, namely, $\mathrm{U}^{u,d}_{L,R}\mathrm{U}^{u,d\dagger}_{L,R}=1$, we note that the interactions with the neutral bosons remain the same in the mass basis. However the charged currents are affected by this change. There for, we define the Cabibbo-Kobayashi-Maskawa (CKM) matrix, as $V_{CKM}=U^u_L U^{u^{\dagger}}_R$ and write the sensitive terms,

$$\mathcal{L}_{kin} \supset \frac{1}{\sqrt{2}}g\bar{u}'_L\gamma^{\mu}V_{CKM}d'_L W^+_{\mu} + h.c. \tag{2.33}$$

The CKM matrix, is a 3×3 unitary matrix. It is a parametrization of the three mixing angles and CP-violating KM phase. There are many possible conventions to represent the CKM matrix. The mixing angles refer to those between the up and down quark families. We can see their hierarchy in Fig. 2.1.

It is through this complex phase in the CKM matrix that the SM can account for the phenomena of $\mathcal{CP}$ violation. First observed in the famous K^0 decay into μ^+ μ^- ($CP=+1$ and $CP=-1$ respectively) [21], that won the 1980 Nobel Prize [22]. The discovery opened the door to questions still at the core of particle physics and of cosmology today. Not just the lack of an exact CP-symmetry, but also the fact that it is so close to a symmetry.

We avoided discussing leptons since in the SM their mass eigenstates can be easily shown to have no real consequence besides a change of basis. We might also note a very interesting feature of the Standard Model, by consequence of the $\mathrm{SU(2)_L}\times\mathrm{U(1)_Y}$ symmetry. There are no interactions of the right handed unitary matrices and thus no mixing, coupling, or charged currents of right handed quarks, making them theoretically invisible to measurements.

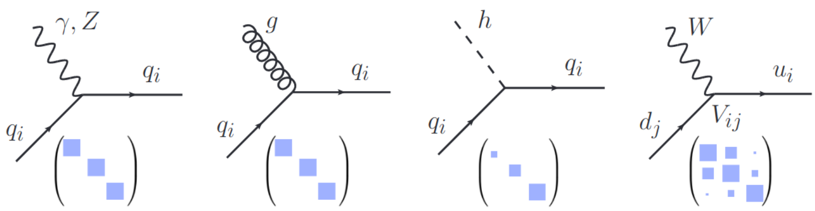

Figure 2.1: Feynman diagrams for flavour conserving couplings of quarks to photon, Z boson, gluon and the Higgs (the first three diagrams), and the flavour changing coupling to the W (the last diagram). The 3×3 matrices are visual representations of couplings in the generation space, with couplings to γ ,Z, g being flavour universal, while the couplings to the Higgs are flavour diagonal but not universal. Finally the couplings involving the W are flavour changing and hierarchical.

The CKM matrix elements are fundamental parameters of the particle physics, so their precise determination is important, and reproducing the quark mixing parameters is fundamental for BSM searches that include changes to how the quarks interact with possible new Higgs bosons.

2.3.1 Charged Flavour Currents vs. Neutral Flavour Currents

In the SM there is a very important distinction between flavour changing neutral and charged currents. FCNCs are processes in which the quark flavour changes, while the quark charge stays the same. The Flavour Changing Charged Currents (FCCCs) change both the flavour and the charge of the quark. Extracting some representative probabilities from [23] reveals that the two types of processes are strikingly different. The charged currents lead to the dominant weak decays, while the FCNCs induce decays that are extremely suppressed. Rounding the experimental results, and not showing the errors, a few representative decays are,

Table 2.4: FCCCs examples

$s \to u\mu^-\nu_\mu$	: Br $\left(K^+ \to \mu^-\nu\right) = 64\%$
$b \to cl^-\nu_l$	: Br $\left(B^- \to D^0 l\bar{\nu}_l\right) = 2.3\%$
$c \to u\mu^-\nu_\mu$	: Br $\left(D^\pm \to K^0\mu^\pm\nu\right) = 9\%$

Table 2.5: FCNCs examples

$s \to d\mu^+\mu^-$	: Br $\left(K_L \to \mu^+\mu^-\right) = 7 \times 10^{-9}$
$b \to d\mu^+\mu^-$	: Br $\left(B^- \to K^{*-}l^+l^-\right) = 5 \times 10^{-7}$
$c \to ul^+l^-$	: Br $\left(D^0 \to \pi l^+l^-\right) = 1.8 \times 10^{-4}$

The reason for such a striking difference is that in the SM the charged currents occur at tree level, while FCNCs are forbidden at tree level and only arise starting at one loop order. Note the lack of neutral couplings between the up and down families in Eq **??**. The relative complexity of these processes can be easily seen in Fig 2.2,

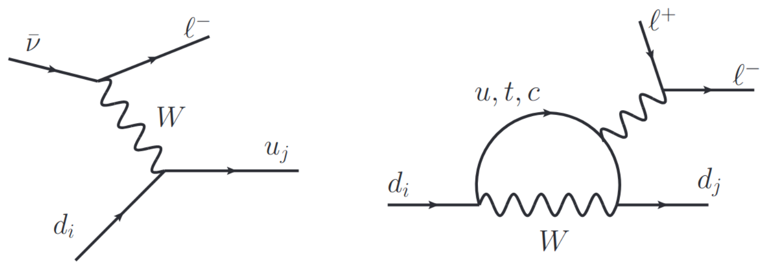

Figure 2.2: Representative tree level charged current diagram (left) and a loop induced FCNC diagram (right).

Furthermore, the FCNCs come suppressed by the difference of the masses of the quarks running in the loop, $m_j^2 - m_i^2$. This so called Glashow-Iliopoulos-Maiani (GIM) mechanism [24]. Given the differences between the masses of the up and down sectors this has a significant impact. A interesting result of this mechanism would be that that there is no flavour violation, if all the quark masses are the same.

Flavour as a Probe into New Physics

Now that we have introduced a small portion of flavour physics we can briefly touch on why collider experiments have been sold as a pathway to discovering new physics i.e. how deviation in rare decays could pin point exactly what is missing in the SM. Thanks to these large experiments we have many new observables in flavour physics, e.g. the branching ratios not coinciding with the SM prediction citation , observed Lepton FLavour Violation in tree and loop levels [25] and others?. For each of these examples there is also a plethora of different parent particles for each change of flavour, as well as many instances of final states. The abundance of observables is clearly illustrated by opening the handy Particle Data Group (PDG) book [23].

The recipe then, seems simple, identify processes that are rare in the SM and then search for deviations from the SM predictions. However, thus far all but two processes are within 2σ experimental and theoretical bounds given by the SM. These are the $b \to s\mu\mu$ and $b \to c\tau\nu$ channels. They are, so far, showing over 4σ deviations from their expected value. (citation needed). Without going into too much depth onto the NP searches, we can examine the scale at which these processes are "integrated away". This is the energy scale at which a NP vector-axial operator would allow these processes to exist only at high energies. These energies are naturally high given the terms in 2.34.

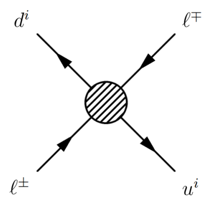

$$\mathcal{L}_{NP} \supset \frac{1}{\Lambda_{NP}}(\overline{Q}_i\gamma^\mu\sigma Q_j)(\overline{L}_k\gamma_\mu\sigma L_l) \tag{2.34}$$

Figure 2.3: "Contact" interactions with loop interactions containing NP

To explain $b \to s\mu\mu$ transitions you would need a $\Lambda_{NP} \approx 3$ TeV while for $b \to c\tau\nu$ you would need a $\Lambda_{NP} \approx 30$ TeV. This is a strong indicator that some components are missing in our formulation like a new mediator for gauge interactions. And the advantage of this scale is it almost certainly in most BSM scenarios, avoiding most experimental constraints.

As for the FCNC diagram, the $b \to s\mu\mu$ channel can be seen in Fig 2.4,

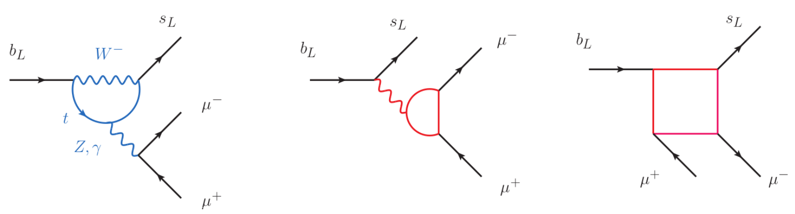

Figure 2.4: A representative SM diagram for $b \to s\mu\mu$ transition (left), and representative possible loop level NP contributions (middle and right).

The $b \to c\tau\nu$ flavour anomaly is similarly very clean theoretically [26]. However, the NP effect in these diagrams is large (citation needed) and often this means that the scale of NP needs to be lower than in the previous case. Consequently the NP interpretations here are often in conflict with experimental constraints (citation needed). This means the most obvious candidates are ruled out. Theoretical bias would have been that the new charged currents are either due to a charged Higgs, H^+ , or a new vector boson, W', see Fig. 2.5 (citation needed).

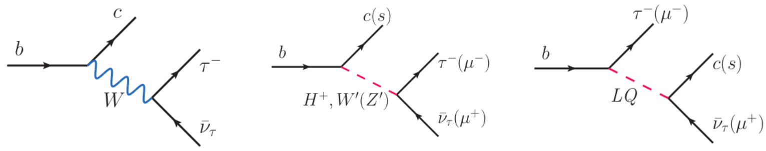

Figure 2.5: The SM diagrams for $b \to c\tau\nu$ transition (left), and the possible tree level NP contributions to $b \to c\tau\nu$ transition (middle and right).

Another prediction of the SM is that the rates for the $b \to se^+e^-$ and $b \to s\mu^-\mu^+$ transitions should be equal to each other. The SM prediction of Lepton Flavour Universality (LFU) is deeply engrained in the structure of the theory, since it is a consequence of the fact that the electroweak gauge group is the same for all three generations. The prediction of LFU can be tested experimentally, also trough flavour physics, by theoretically clean observables such as the ratios of these flavour observables,

$$R_{K^*} = \frac{\mathrm{Br}(B \to K^*\mu^-\mu^+)}{\mathrm{Br}(B \to K^*e^-e^+)} \tag{2.35}$$

Another strong indicator of new physics is the fact the experimental value for this ratio is $R_{K^*} \approx 0.7$, violating LFU by $2.2 - 2.6\sigma$ (citation needed).

The Future of Flavour Indirect Searches

The NP searches with rare decays, will benefit from the upcoming upgrades at Belle II and the LHC. Belle II expects to collect 50 times the Belle dataset. First collisions were seen in May 2018, and the first B physics run is expected in March 2019. While for the LHC, after upgrade II aims for roughly 100 times the present data set with an upgraded detector. (citation needed). Undoubtedly this improvement in sensibility will translate to a finer value for all measurable parameters at these experiments. We expect these anomalies then to go over the required 5σ in future experiments (Assuming of course, they are not statistical deviations). (citation needed).

Chapter 3

B-L-SM Model

Here we start the our first look at BSM scenarios. In this chapter we introduce the minimal $\mathrm{U(1)_{B-L}}$ gauge extension of the Standard Model named, the B-L-SM Model [27, 28, 29]. This is a model trough which we can explain neutrino mass generation via a simple see-saw mechanism, additionally, by virtue of the model containing two new physical particle states, specifically a new Higgs like boson $\mathrm{H'}$ and a $\mathrm{Z'}$ gauge Boson we can also address other phenomenology, such as deviations in electro-weak measurements, namely the $(g-2)_\mu$ anomaly. The discrepancy between the measured anomalous magnetic moment of the muon and the SM expected value [30].

Both the additional bosons are given mass primarily trough the spontaneous breaking of the $\mathrm{U(1)_{B-L}}$ symmetry that gives it's name to the Model. This unitary group originates from the promotion of a accidental symmetry present in the SM, the Baryon number (B) minus the Lepton number (L) to a fundamental Abelian symmetry group. This origin for the mass of the referenced bosons means model is already very heavily constricted due to long-standing direct searches in the Large Hadron Collide (LHC).

Trough this model we can address the metastability of the electroweak (EW) vacuum in the SM trough the new scalar. Allowing for Higgs stabilization up to the plank scale with a the new Higgs starting from few hundred of GeVs [31, 32, 33].

The B-L-SM is particular interesting in the context of the study of Grand Unified Theories (GUT) as it easily embedded into higher order symmetry groups like for example the SO(10) [34, 35, 36, 37, 38] or $\mathrm{E_6}$ [39, 40, 41].

The presence of a new complex singlet field, χ, with a (tradicional) Higgs doublet typically results in enhanced strength of the EW phase transition potentially converting it into a strong first-order one, this would be could be detectable in the form of a gravitational wave background [42]. Such a analysis is of utmost importance given that it could provide a way to detect NP or exclude models without the need for a larger particle collider but instead a sensitive probe also capable of studying gravitational events.

However a family-universal symmetry such as $\mathrm{U(1)_{B-L}}$ being introduced without changing the SM fermion content would lead to chiral anomalies. This translates to a non conservative charged current on some channels involving the $\mathrm{U(1)_{B-L}}$. These aren't completely undesired by themselves, since their result would be charge conjugation parity symmetry violation, but this inclusion at tree-level without a suppression mechanism would lead to far too much $\mathcal{CP}$ violation.

The model also benefits from presence of three generations of right-handed heavy Majorana neutrinos that trough the new field additions are possible in a framework free of anomalies while also enabling a minimal see-saw mechanism to generate light neutrino masses unlike the SM. [43, 44, 45].´ The mass scale of such neutrinos is established once the $\mathrm{U(1)_{B-L}}$ symmetry is broken. These neutrinos are of cosmological significance given their presence could imply the existence of a sterile state that can play the role of Dark Matter candidate [46]. The relatively small alteration of a, $\mathbb{Z}_2$, symmetry in the neutrino sector can make these fully sterile, as seen in [47, 48]. Check if the Z2 affects the Zprime, if so we must comment that it doens't allow kinetic mixing! and would alter the a_μ These neutrinos can, in such case, be used to help explain the baryon asymmetry via the leptogenesis mechanism, this scenario is discussed in depth in the following Refs. [49, 50, 51].

The structure of this chapter is to first present the fundamental theoretical background on the model with a strong focus on the basic details of scalar and gauge boson mass spectra and mixing. Followed by a modern precise study of the phenomenological status of the B-L-SM model trough a layered algorithm that will be discussed preceding the results. Through this algorithm we provide a numerical analysis that tests the relevant phenomenological constraints in direct and electroweak observables. Followed by this study we table of a few representative benchmark points to be possibly tested in by experiments.

perhaps I should include this on the start of the chapter

3.1 Formulating the model

Essentially, the minimal B-L-SM is a BSM framework containing only three new ingredients, a new gauge interaction given the new symmetry group, three generations of right handed neutrinos, and a complex scalar field χ.

The first of these, is motivated by the aforementioned GUT scenarios, as seen in the Refs, [34, 35, 36, 37, 38, 39, 40, 41], here you can see that the B-L-SM can be introduced in a large number of groups, like E_6 and SO(10).

Secondly, as mentioned, a new sector of additional three $U(1)_{B-L}$ charged Majorana neutrinos is essential for anomaly cancellation and addresses many concerns of the SM.

Finally, the SM-like Higgs doublet, H, does not carry neither baryon nor lepton number, this way it does not participate in the breaking of $U(1)_{B-L}$. It is then necessary to introduce a new scalar singlet field, χ, solely charged under $U(1)_{B-L}$, to perform the breaking of the $B-L$ symmetry.

The particle content and related charges of the minimal $U(1)_{B-L}$ extension of the SM are shown in the table. Note these are similar to the SM as to be expected.

	q_L	u_R	d_R	l_L	e_R	ν_R	H	χ
$SU(3)_c$	3	3	3	1	1	1	1	1
$SU(2)_L$	2	1	1	2	1	1	2	1
$U(1)_Y$	$\frac{1}{6}$	$\frac{2}{3}$	-$\frac{1}{3}$	-$\frac{1}{2}$	-1	0	$\frac{1}{2}$	0
$U(1)_{B-L}$	$\frac{1}{3}$	$\frac{1}{3}$	$\frac{1}{3}$	-1	-1	-1	0	2

Table 3.1: Quantum fields and their respective quantum numbers in the minimal B-L-SM extension. The last two lines represent the weak and $B-L$ hypercharges

Scalar sector

Given the information seen above, we can begin examining the new Lagrangian terms. Starting by the scalar potential, which now depends on two fields as seen in,

$$V(H,\chi) = \mu_1^2 H^\dagger H + \mu_2^2 \chi^* \chi + \lambda_1 (H^\dagger H)^2 + \lambda_2 \left(\chi^* \chi\right)^2 + \lambda_3 \chi^* \chi H^\dagger H \tag{3.1}$$

Being, λ_i, the scalar couplings. This potential must lead to stable vacuum state, for this the scalar potential must be bounded from below (BFB), as to ensure a global minima. Studying the potential on eq. 3.1 we deduce the conditions,

$$4\lambda_1\lambda_2 - \lambda_3^2 > 0 \quad , \quad \lambda_1, \lambda_2 > 0 \tag{3.2}$$

Where the full components of the scalar fields H and χ are given by,

$$H = \frac{1}{\sqrt{2}} \begin{pmatrix} -i\left(\omega_1 - i\omega_2\right) \\ v + (h + iz) \end{pmatrix} \qquad \chi = \frac{1}{\sqrt{2}} \left(x + (h' + iz')\right) \tag{3.3}$$

In these equations we can see h and h' representing the radial quantum fluctuations around the minimum of the potential. These will constitute the physical degrees of freedom associated to the H and H'. There are also four Goldstone directions denoted as ω_1, ω_2, z and z' which are absorbed into longitudinal modes of the $W^{\pm}$, Z and Z' gauge bosons once spontaneous symmetry breaking (SSB) takes place. After SSB the associated VEVs take the form,

$$\langle H \rangle = \frac{1}{\sqrt{2}} \begin{pmatrix} 0 \\ v \end{pmatrix} \qquad \langle \chi \rangle = \frac{x}{\sqrt{2}} \tag{3.4}$$

From here we can solve the tadpole equations in relation to each of the VEVs as to ensure non-zero VEV, we arrive at,

$$v^2 = \frac{-\lambda_2 \mu_1^2 + \frac{\lambda_3}{2}\mu_2^2}{\lambda_1\lambda_2 - \frac{1}{4}\lambda_3^2} > 0 \qquad \text{and} \qquad x^2 = \frac{-\lambda_1 \mu_2^2 + \frac{\lambda_3}{2}\mu_1^2}{\lambda_1\lambda_2 - \frac{1}{4}\lambda_3^2} > 0 \tag{3.5}$$

which, when simplified with the bound from bellow conditions yield a simpler set of equations,

$$\lambda_2 \mu_1^2 < \tfrac{\lambda_3}{2}\mu_2^2 \qquad \text{and} \qquad \lambda_1 \mu_2^2 < \tfrac{\lambda_3}{2}\mu_1^2 \tag{3.6}$$

Note that although λ_1 and λ_2 must be positive to ensure the correct conical shape to the potential, no such conditions exist for the sign of λ_3 , μ_1, and μ_2. However observing equation 3.6 we can infer that only some combinations of signs are impossible,

	$\mu_2^2 > 0$, $\mu_1^2 > 0$	$\mu_2^2 > 0$, $\mu_1^2 < 0$	$\mu_2^2 < 0$, $\mu_1^2 > 0$	$\mu_2^2 < 0$, $\mu_1^2 < 0$
$\lambda_3 < 0$	✗	✓	✓	✓
$\lambda_3 > 0$	✗	✗	✗	✓

Table 3.2: Possible Signs of the potential parameters in (3.1). While the ✓ symbol indicates the existence of solutions for tadpole conditions (3.6), the ✗ indicates unstable configurations.

For our numerical analysis we decided to leave the sign of λ_3 positive, choosing a configuration where both μ parameters are negative. This doesn't directly translate to any real physical consequence. These conditions now established we proceed to investigate the physical states of B-L-SM scalar sector. By first, taking the Hessian matrix evaluated at the vacuum value,

$$\mathbf{M}^2 = \begin{pmatrix} 4\lambda_2 x^2 & \lambda_3 v x \\ \lambda_3 v x & 4\lambda_1 v^2 \end{pmatrix}, \tag{3.7}$$

Moving this matrix to it's physical mass eigen-base, we obtain the following eigenvalues,

$$m_{h_{1,2}}^2 = \lambda_1 v^2 + \lambda_2 x^2 \mp \sqrt{(\lambda_1 v^2 - \lambda_2 x^2)^2 + (\lambda_3 x v)^2}\,, \tag{3.8}$$

The physical basis vectors h_1 and h_2 can then be related to the original fields of gauge eigen-basis h and h' trough a simple rotation matrix:

$$\begin{pmatrix} h_1 \\ h_2 \end{pmatrix} = \mathbf{O} \begin{pmatrix} h \\ h' \end{pmatrix}. \tag{3.9}$$

Being that, the rotation matrix is written as,

$$\mathbf{O} = \begin{pmatrix} \cos\alpha_h & -\sin\alpha_h \\ \sin\alpha_h & \cos\alpha_h \end{pmatrix}. \tag{3.10}$$

The precise mixing angle is represented simply by,

$$\tan 2\alpha_h = \frac{|\lambda_3|\, vv'}{\lambda_1 v^2 - \lambda_2 v'^{\,2}} \tag{3.11}$$

Although consider it is worth presenting the case of approximate decoupling where, $v/x \ll 1$. In this case scalar masses and mixing angle become particularly simple,

$$\sin\alpha_h \approx \frac{1}{2}\frac{\lambda_3}{\lambda_2}\frac{v}{x} \qquad m_{h_1}^2 \approx 2\lambda_1 v^2 \qquad m_{h_2}^2 \approx 2\lambda_2 x^2 \tag{3.12}$$

We will see in the context of our numerical results that for our phenomenologically consistent mass scale these equations serve a valid approximation for most of the points.

Gauge Sector

Moving onto the gauge boson and Higgs kinetic terms in the B-L-SM, consider the following portion of the Lagrangian,

$$\mathcal{L}_{U(1)'s} = |D_\mu H|^2 + |D_\mu \chi|^2 - \frac{1}{4}F_{\mu\nu}F^{\mu\nu} - \frac{1}{4}F'_{\mu\nu}F'^{\mu\nu} - \frac{1}{2}\kappa F_{\mu\nu}F'^{\mu\nu} \tag{3.13}$$

where $F^{\mu\nu}$ and $F'^{\mu\nu}$ are the standard field strength tensors, respectively for the hypercharge $\mathrm{U(1)_Y}$ and B minus L $\mathrm{U(1)_{B-L}}$,

$$F_{\mu\nu} = \partial_\mu A_\nu - \partial_\nu A_\mu \qquad \text{and} \qquad F'_{\mu\nu} = \partial_\mu A'_\nu - \partial_\nu A'_\mu\,. \tag{3.14}$$

written in terms of the gauge fields A_μ and A'_μ, respectively. Given that this is a model with two Unitary groups, without a parity symmetry ($\mathbb{Z}_2$) to prevent it, we must consider the possible mixing in between them. In this work we parametrized this mixing trough a parameter κ.

The Abelian part of the covariant derivative in equation 3.13 is given by,

$$D_\mu \supset i g_1 Y A_\mu + i g'_1 Y_{\mathrm{B-L}} A'_\mu\,, \tag{3.15}$$

with g_1 and g'_1 being the $\mathrm{U(1)_Y}$ and $\mathrm{U(1)_{B-L}}$ the gauge couplings with the Y and $B-L$ charges are specified in Tab. 3.1. However it is convenient to rewrite the gauge kinetic terms in the canonical form, i.e.

$$F_{\mu\nu}F^{\mu\nu} + F'_{\mu\nu}F'^{\mu\nu} + 2\kappa F_{\mu\nu}F'^{\mu\nu} \to B_{\mu\nu}B^{\mu\nu} + B'_{\mu\nu}B'^{\mu\nu}\,. \tag{3.16}$$

A generic orthogonal transformation in the field space does not eliminate the kinetic mixing term. So, in order to satisfy Eq. (3.16) an extra non-orthogonal transformation should be imposed such that Eq. (3.16) is realized. Taking $\kappa = \sin\alpha$, a suitable redefinition of fields $\{A_\mu, A'_\mu\}$ into $\{B_\mu, B'_\mu\}$ that eliminates κ-term according to Eq. (3.13) can be cast as

$$\begin{pmatrix} A_\mu \\ A'_\mu \end{pmatrix} = \begin{pmatrix} 1 & -\tan\alpha \\ 0 & \sec\alpha \end{pmatrix} \begin{pmatrix} B_\mu \\ B'_\mu \end{pmatrix}, \tag{3.17}$$

Note there is a limit without kinetic mixing where $\alpha = 0$. Note that this transformation is generic and valid for any basis in the field space. The transformation (3.17) results in a modification of the covariant derivative that acquires two additional terms encoding the details of the kinetic mixing, i.e.

$$D_\mu \supset \partial_\mu + i\,(g_Y\, Y + g_B Y\, Y_{B-L})\, B_\mu + i\,(g_{B-L}\, Y_{B-L} + g_{YB}\, Y)\, B'_\mu\,, \tag{3.18}$$

where the gauge couplings take the form

$$\begin{cases} g_Y = g_1 \\ g_{B-L} = g'_1 \sec\alpha \\ g_{YB} = -g_1 \tan\alpha \\ g_{BY} = 0 \end{cases}, \tag{3.19}$$

which is the standard convention in the literature. Note this definition is merely to simply the equations and has no physical impact. We will later see that this kinetic mixing is a desired feature and why stabilizing it with a $\mathbb{Z}_{\not{\varepsilon}}$ symmetry would be detrimental in terms of depth. The resulting mixing between the neutral gauge fields including Z' can be represented as follows

$$\begin{pmatrix} \gamma_\mu \\ Z_\mu \\ Z'_\mu \end{pmatrix} = \begin{pmatrix} \cos\theta_W & \sin\theta_W & 0 \\ -\sin\theta_W \cos\theta'_W & \cos\theta_W \cos\theta'_W & \sin\theta'_W \\ \sin\theta_W \sin\theta'_W & -\cos\theta'_W \sin\theta'_W & \cos\theta'_W \end{pmatrix} \begin{pmatrix} B_\mu \\ A^3_\mu \\ B'_\mu \end{pmatrix} \tag{3.20}$$

where θ_W is the weak mixing angle and θ'_W is defined as

$$\sin(2\theta'_W) = \frac{2g_{YB}\sqrt{g^2+g_Y^2}}{\sqrt{(g_{YB}^2 + 16(\frac{x}{v})^2 g_{B-L}^2 - g^2 - g_Y^2)^2 + 4g_{YB}^2(g^2+g_Y^2)}}\,, \tag{3.21}$$

in terms of g and g_Y being the $SU(2)_L$ and U_Y gauge couplings, respectively. In the physically relevant limit, $v/x \ll 1$, the above expression greatly simplifies leading to

$$\sin\theta'_W \approx \frac{1}{16}\frac{g_{YB}}{g_{B-L}}\left(\frac{v}{x}\right)^2 \sqrt{g^2+g_Y^2}\,, \tag{3.22}$$

up to $(v/x)^3$ corrections. In the limit of no kinetic mixing, i.e. $g_{YB} \to 0$, there is no mixture of Z' and SM gauge bosons.

Note, the kinetic mixing parameter θ'_W has rather stringent constraints from Z pole experiments both at the Large Electron-Positron Collider (LEP) and the Stanford Linear Collider (SLC), restricting its value to be smaller than 10^{-3} approximately, which we set as an upper bound in our numerical analysis. Expanding the kinetic terms $|D_\mu H|^2 + |D_\mu \chi|^2$ around the vacuum one can extract the following mass matrix for vector bosons

$$m_V^2 = \frac{v^2}{4}\begin{pmatrix} g^2 & 0 & 0 & 0 & 0 \\ 0 & g^2 & 0 & 0 & 0 \\ 0 & 0 & g^2 & -gg_Y & -gg_{YB} \\ 0 & 0 & -gg_Y & g_Y^2 & g_Y g_{YB} \\ 0 & 0 & -gg_{YB} & g_Y g_{YB} & g_{YB}^2 + 16\left(\frac{x}{v}\right)^2 g_{B-L}^2 \end{pmatrix} \tag{3.23}$$

whose, first set eigenvalues read,

$$m_A = 0\,, \qquad m_W = \tfrac{1}{2}vg \tag{3.24}$$

corresponding to the expected physical photon and $W^\pm$ bosons. While the following set,

$$m_{Z,Z'} = \sqrt{g^2+g_Y^2}\cdot\frac{v}{2}\sqrt{\frac{1}{2}\left(\frac{g_{YB}^2 + 16(\frac{x}{v})^2 g_{\mathrm{BL}}^2}{g^2+g_{\mathrm{Y}}^2}+1\right) \mp \frac{g_{YB}}{\sin(2\theta'_W)\sqrt{g^2+g_{\mathrm{Y}}^2}}}\,. \tag{3.25}$$

correspond to two neutral massive vector bosons, with one of them, not necessarily the lightest, representing the SM-like Z boson. It follows from LEP and SLC constraints on θ'_W, that Eq. (3.22) also implies that either g_{YB} or the ratio $\frac{v}{x}$ are small. In this limit, Eq. (3.25) simplifies to

$$m_Z \approx \tfrac{1}{2}v\sqrt{g^2+g_Y^2} \qquad \text{and} \qquad m_{Z'} \approx 2g_{B-L}x\,, \tag{3.26}$$

where the $m_{Z'}$ depends only on the SM-singlet VEV ,x and on the $\mathrm{U(1)_{B-L}}$ gauge coupling and will be attributed to a heavy Z' state, while the light Z-boson mass corresponds to its SM value.

The Yukawa sector

One of the key features of the B-L-SM is the presence of non-zero neutrino masses. In its minimal version, such masses are generated via a type-I seesaw mechanism, thus producing a very light neutrino for each of the three known neutrino flavours, and a corresponding very heavy neutrino for each, which has yet to be observed. In the type-I seesaw mechanism the mixing of neutrinos fields is written with similar shape to,

$$\left(\begin{array}{c|c} 0 & A \\ \hline A & B \end{array}\right) \tag{3.27}$$

This system would have a set eigenvalues written as,

$$\lambda_{\pm} = \frac{B \pm \sqrt{B^2 + 4A}}{2} \tag{3.28}$$

Investigating the nature of this set of eigenvalues allows us to understand the see-saw. The mean of these values being always equal to $|B|$, if one value goes up, another goes down, like a see-saw. Note B, generally is the Majorana mass terms, and is generally very large in comparison to the cross interaction terms. Given this the smaller eigenstate to be approximate,

$$\lambda_{-} \approx \frac{A^2}{B} \tag{3.29}$$

This mechanism serves to explain why the neutrino masses are so small.

The total Yukawa Lagrangian of the model reads,

$$\mathcal{L}_f = -Y_u^{ij}\overline{q_{\mathrm{Li}}}u_{\mathrm{Rj}}\widetilde{H} - Y_d^{ij}\overline{q_{\mathrm{Li}}}d_{\mathrm{Rj}}H - Y_e^{ij}\overline{\ell_{\mathrm{Li}}}e_{\mathrm{Rj}}H - Y_\nu^{ij}\overline{\ell_{\mathrm{Li}}}\nu_{\mathrm{Rj}}\widetilde{H} - \frac{1}{2}Y_\chi^{ij}\overline{\nu^c_{\mathrm{Ri}}}\nu_{\mathrm{Rj}}\chi + \text{c.c.} \tag{3.30}$$

Notice the explicit lack of Majorana neutrino mass terms of the form $M\overline{\nu_R^c}\nu_R$. These explicitly violate the $\mathrm{U}(1)_{\mathrm{B-L}}$ symmetry and are therefore not present. In Eq. (3.30), Y_u, Y_d and Y_e are the 3×3 Yukawa matrices that reproduce the quark and charged lepton sector exactly the same way as in the SM, while Y_ν and Y_χ are the new Yukawa matrices responsible for the generation of right handed neutrino masses and mixing with left handed fields. In particular, one can write,

$$\mathbf{m}_{\nu_l}^{Type-I} = \frac{1}{\sqrt{2}}\frac{v^2}{x}\mathbf{Y}_\nu^t \mathbf{Y}_\chi^{-1}\mathbf{Y}_\nu \,, \tag{3.31}$$

for light ν_l neutrino masses, whereas the heavy ν_h ones are given by

$$\mathbf{m}_{\nu_h}^{Type-I} \approx \frac{1}{\sqrt{2}}\mathbf{Y}_\chi x \,, \tag{3.32}$$

where we have assumed a flavour diagonal basis.

Note that the smallness of light neutrino masses imply that either the x VEV is very large or (if we fix it to be at the $\mathcal{O}(TeV)$ scale and $\mathbf{Y}_\chi \sim \mathcal{O}(1)$) the corresponding Yukawa coupling should be tiny, $\mathbf{Y}_\nu < 10^{-6}$. It is clear that the low scale character of the type-I seesaw mechanism in the minimal B-L-SM is *faked* by small Yukawa couplings to the Higgs boson. A more elegant description was proposed in Ref. [52] where small SM neutrino masses naturally result from an inverse seesaw mechanism. In this work, however, we will not study the neutrino sector and thus, for an improved efficiency of our numerical analysis of Z' observables, it will be sufficient to fix the Yukawa couplings to $\mathbf{Y}_\chi = 10^{-1}$ and $\mathbf{Y}_\nu = 10^{-7}$ values such that the three lightest neutrinos lie in the sub-eV domain.

I think I should show more of the diagonalization process? This last part seems barren

3.2 Numerical Results

Before we begin this section consider that our colleges in a recent work tested the state of the art at the LHC for low mass Z' boson [53]. In particular from 0.2GeV to 200GeV. As for slightly heavier Z' masses beyond $m_{Z'} \gtrsim 100$ GeV, the combined effect of the electroweak precision observables and the ATLAS searches for Drell-Yan Z' production decaying into di-leptons, i.e. $pp \to Z' \to ee, \mu\mu$ [54], is also finely investigated. We then endeavoured to achieve a complementary study where we investigated the case of very heavy Z' bosons.

Our goal was to discover if it was still possible to, with such a heavy Z' boson, limited by LHC, with such a heavily constrained kinetic mixing, to have any significant phenomenological impact asides from simply a yet to be observed boson. This was chiefly done by the investigation of the $(g-2)_\mu$ anomaly. We examine the relations that this anomaly has with the parameter space, such as gauge couplings, as well as the extra scalar mass. The $(g-2)_\mu$ anomaly refers to the discrepancy between the measured anomalous magnetic moment of the muon, $a_\mu^{\text{exp}} \equiv \frac{1}{2}(g-2)_\mu^{\text{exp}}$, and its theoretical prediction, $a_\mu^{\text{SM}} \equiv \frac{1}{2}(g-2)_\mu^{\text{SM}}$, which reads [30]

$$\Delta a_\mu = a_\mu^{\text{exp}} - a_\mu^{\text{SM}} = 268(63)(43) \times 10^{-11} \tag{3.33}$$

with numbers in brackets denoting experimental and theoretical errors, respectively. This represents a tension of 3.5 standard deviations from the combined 1σ error and is calling for new physics effects beyond the SM theory.

There is a strong possibility that through radiative corrections a new gauge bosons could explain this deviation [55]. In fact a version of this study has already been performed in the supersymmetrical version of the B-L-SM [56, 57].

3.2.1 The scanning apparatus

The numerical data presented in this section of our work was generated thorough a large chain of nested scripts. These were created as a possible first generation of a scanning framework for generic phenomenological models. This machinery was adapted to the 3HDM numerical scan so this introduction will be glossed over in the 3HDM section, as much remained the same.

The scripts were a mixture of Linux bash and Python 3 scripts, and utilize the `SPheno 4.0.3` [58, 59], `SARAH 4.13.0` [60, 61], `HiggsBounds 4.3.1` [62], `HiggsSignals 1.4.0` [63] and `MadGraph5_aMC@NLO 2.6.2` [64] programs/packages.

These scripts generate a Monte-Carlo type scan through a desired parameter space. Unless introduced, all non-relevant physical constants and parameters are defined in a way as to keep the observed gauge, lepton and quark structure consistent with the SM. Skipping a bit ahead, as a example, for the B-L-SM scan our scanning routine randomly samples parameter space points according to the ranges in Tab. 3.3 while keeping things like Higgs doublet VEV and Weinberg angle to reproduce the correct W and Z structure.

Given the randomness in our scan, we can reach unphysical, or nonsensical regions, that contain objects like tachyonic scalar masses un-renormalizable quantities, divergent radiative corrections etc. These points must be rejected before even considering experimental constraints. This is done by `SPheno`, rejecting any point generated with unphysical parameters.

We could consider this our first layered check. While a second layer of tests include the phenomenological studies we shall perform. This is the region where we confront the surviving scenarios with experimental data. Such as precision measurements from the oblique S, T, U parameters and constraining the Higgs Sector to reproduce the observed signal seen in the LHC in 2012. The latter is made automatically trough the package `HiggsBounds 4.3.1` that shall be used to apply a 95% C.L. exclusion limit cut on a new scalar particle, h_2, while `HiggsSignals 1.4.0` is used to calculate and later check, through a χ^2 distribution, the probability for consistency with the observed Higgs boson signal data. To calculate these variables `HiggsBounds 4.3.1` and `HiggsSignals 1.4.0` are provided all scalar masses, total decay widths, Higgs decay branching ratios as well as the SM-normalized effective Higgs couplings to fermions and bosons squared (that are needed for analysis of the Higgs boson production cross sections). For details about this calculation, see Ref. [62].

All data generated for a point in the parameter space is generated by `SPheno`. `SPheno` is a particle spectrum generator code written in Fortran 90. It's emphasis on easy generalisability and speed made it a natural part of our numerical analysis. It takes information about our models Lagrangian, such as fields, charges and fundamental symmetries, and creates a executable file capable of quickly generating a spectrum file with all details regarding mass, decay and flavour observables information in the standardized SUSY Les-Houches accord format. All generated spectrums are processed and stored. This Lagrangian information is fed to `SPheno` also in standardized format automatically generated by a Mathematica packaged designed for such purposes called `SARAH`.

On a third and final layer of phenomenological tests we have studied the viability of the surviving scenarios from the perspective of direct collider searches for a new Z' gauge boson. We have used, the popular `MadGraph5_aMC@NLO`, to compute the Z' Drell-Yan production cross section and subsequent decay into the first and second-generation leptons, i.e. $\sigma\,(pp \to Z') \times B\,(Z' \to \ell\ell)$ with $\ell = e,\ \mu$, and then compared our results to the most recent ATLAS exclusion bounds from the LHC runs at the center-of-mass energy $\sqrt{s} = 13$ TeV [54]. The `SPheno` SLHA output files were used as parameter cards for `MadGraph5_aMC@NLO`, where the information required to calculate $\sigma\,(pp \to Z') \times B\,(Z' \to \ell\ell)$, such as the Z' boson mass, its total width and decay branching ratios into lepton pairs, is provided. The lepton anomalous magnetic moments $(g-2)_\ell/2 \equiv a_\ell$ are calculated in `SPheno` at one-loop order. In the B-L-SM, new physics (NP) contributions to a_μ, denoted as $\Delta a_\mu^{\mathrm{NP}}$ in what follows, can emerge from the diagrams containing Z' or h_2 propagators, as a example consider Figs. 3.3.

3.2.2 Numerical discussion

For the B-L-SM scan our scanning routine randomly samples parameter space points according to the ranges in Tab. 3.3.

λ_1	$\lambda_{2,3}$	$g_{\mathrm{B-L}}$	g_{YB}	x [TeV]
$[10^{-2},\ 10^{0.5}]$	$[10^{-8},\ 10]$	$[10^{-8},\ 10]$	$[10^{-8},\ 10]$	$[0.5,\ 20.5]$

Table 3.3: Parameter scan ranges used in our analysis. Note that the value of λ_1 is mostly constrained by the tree-level Higgs boson mass given in Eq. (3.12).

Keeping the remaining free parameters of the model to be in agreement with the Standard Model. The presence of new bosons in the theory can lead to large deviations in EW precision observables. Typically, the most stringent constraints of the scalar sector emerge from the oblique S, T, U parameters, which are also calculated by `SPheno`. Current precision measurements provide the allowed regions,

$$S = 0.02 \pm 0.10\,, \qquad T = 0.07 \pm 0.12\,, \qquad U = 0.00 \pm 0.09 \tag{3.34}$$

where S-T are 92% correlated, while S-U and T-U are -66% and -86% anti-correlated, respectively. We compare our results with the EW fit in Eq. (3.34) and require consistency with the best fit point within a 95% C.L. ellipsoid (see Ref. [65] for further details about this method). We show in Fig. 3.1 our results in the ST (left) and TU (right) planes where black points are consistent with EW precision observables at 95% C.L. whereas grey ones lie outside the corresponding ellipsoid of the best fit point and, thus, the first points to be excluded in our analysis.

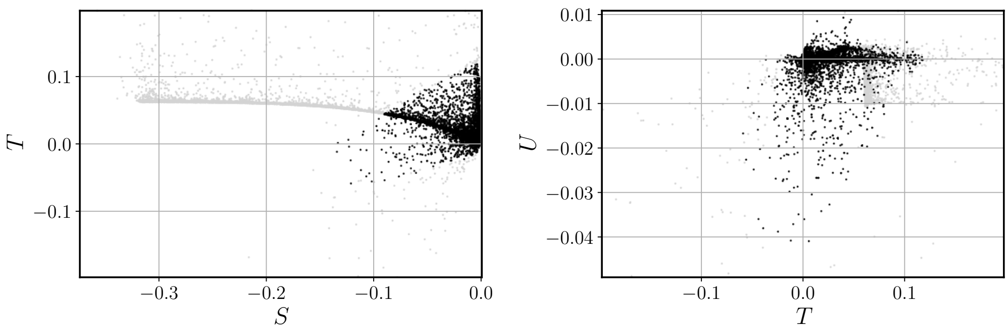

Figure 3.1: Scatter plots for EW precision observables showing the ST (left) and TU (right) planes. Accepted points lying within a 95% C.L. ellipsoid of the best fit point are represented in black whereas grey points are excluded.

As stated we confront the surviving scenarios, black points in Fig. 3.1, with collider bounds. In particular 95% C.L. exclusion limits on a new scalar particle and check for consistency with the observed Higgs boson at 3σ. From here we move onto the third layer of phenomenological tests we have studied the viability of the surviving scenarios from the perspective of direct collider searches for a new Z' gauge boson at the most recent collider experiments. Let us now discuss the phenomenological properties of the B-L-SM model. First, we focus on the current collider constraints and study their impact on both the scalar and gauge sectors.

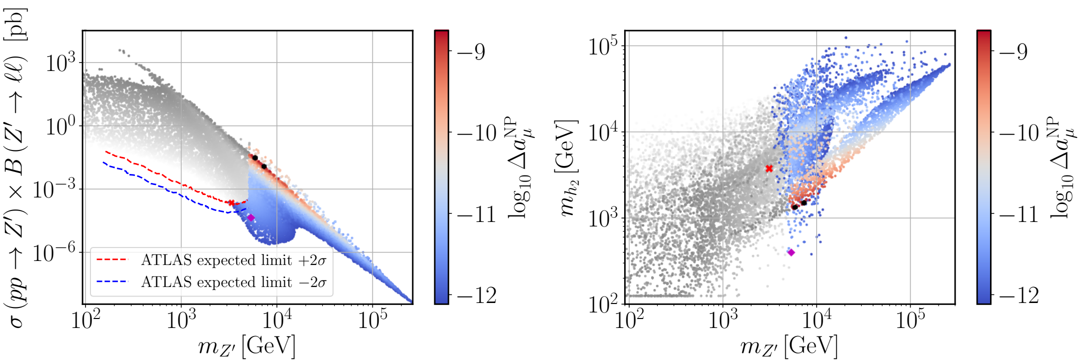

Figure 3.2: Scatter plots showing the Z' Drell-Yan production cross section times the decay branching ratio into a pair of electrons and muons (left panel) and the new scalar mass m_{h_2} (right panel) as functions of $m_{Z'}$ and the new physics (NP) contributions to the muon Δa_μ anomaly. Coloured points have survived all theoretical and experimental constraints while grey points are excluded by direct Z' searches at the LHC. The region between the two dashed lines represents the current ATLAS expected limit on the production cross section times branching ratio into a pair of leptons at 95% C.L. and is taken from the *Brazilian* plot in Fig. 4 of Ref. [54]. The four highlighted points in both panels denote the benchmark scenarios described in detail in Tab. 3.4.

We show in Fig. 3.2 the scenarios generated in our parameter space scan (see Tab. 3.3) that have passed all theoretical constraints such as boundedness from below, unitarity and EW precision tests, are compatible with the SM Higgs data and where a new visible scalar h_2 is unconstrained by the direct collider searches. On the left panel, we show the Z' production cross section times its branching ratio to the first- and second-generation leptons, $\sigma B \equiv \sigma\,(pp \to Z') \times B\,(Z' \to \ell\ell)$ with $\ell = e, \mu$, as a function of the new vector boson mass and the new physics contribution to the muon anomalous magnetic moment $\Delta a_\mu^{\rm NP}$ (colour scale). On the right panel, we show the new scalar mass as a function of the same observables. All points above the red dashed line are excluded at

95% C.L. by the upper expected limit on Z' direct searches at the LHC by the ATLAS experiment and are represented in grey shades. Darker shades denote *would-be-scenarios* with larger values of $\Delta a_\mu^{\rm NP}$ while the smaller contributions to the muon $(g-2)_\mu/2$ anomaly are represented with the lighter shades. The region between the two dashed lines corresponds to the Z' ATLAS limit with a 2σ uncertainty represented by the yellow band in Fig. 4 of [54]. Provided that the observed limit by the ATLAS detector lies within this region we have taken a conservative approach and accepted all points whose σB value lies below the red dashed line (upper limit) in Fig. 3.2. The blue dashed line, which corresponds to the stricter 2σ lower bound, is only shown for completeness of information. The red cross in our figures signals the lightest Z' found in our scan which we regard as a possible early-discovery (or early-exclusion) benchmark point in the forthcoming LHC runs. Such a benchmark point is shown in the first line of Tab. 3.4. On the right panel, we notice that the new scalar bosons can become as light as $380-400$ GeV, but with Z' masses in the range of $5-9$ TeV. We highlight with a magenta diamond the benchmark point with the lightest Z' boson within this range. This point is shown in the second line of Tab. 3.4.

$m_{Z'}$	m_{h_2}	x	$\log_{10}\Delta a_\mu^{\rm NP}$	σB	θ'_W	α_h	$g_{\text{B-L}} \simeq g^{\ell\ell Z'}$
3.13	3.72	15.7	-12.1	2.22×10^{-4}	≈ 0	5.67×10^{-5}	0.0976
5.37	0.396	9.10	-11.7	4.23×10^{-5}	2.55×10^{-7}	9.44×10^{-7}	0.302
7.35	1.49	0.321	-8.75	0.0115	1.83×10^{-7}	1.20×10^{-6}	3.15
5.91	1.32	0.335	-8.78	0.0285	1.30×10^{-4}	1.04×10^{-5}	2.94

Table 3.4: A selection of four benchmark points represented in Figs. 3.2, 3.4 to 3.6. The $m_{Z'}$, m_{h_2} and x parameters are given in TeV. The first line represents a point with light h_2 while the second line shows the lightest allowed Z' boson found in our scan. The last two lines show two points that reproduce the observed value of the muon $(g-2)$ within 1σ uncertainty.

Implications of direct Z' searches at the LHC for the $(g-2)_\mu$ anomaly

Looking again to Fig. 3.2 (left panel), we see that there is a thin dark-red stripe where $\Delta a_\mu^{\rm NP}$ explains the observed anomaly shown in Eq. (3.33) for a range of $m_{Z'}$ boson masses approximately between 5 TeV and 20 TeV. This region is particularly interesting as it can be partially probed by the forthcoming LHC runs or at future colliders. If a Z' boson discovery remains elusive for such a mass range, it can exclude a possibility of explaining the muon $(g-2)_\mu$ anomaly in the context of the B-L-SM. It is also worth noticing that such preferred $\Delta a_\mu^{\rm NP}$ values represent a small island in the right plot of Fig. 3.2 where the new scalar boson mass is restricted to the range of $1~\text{TeV} < m_{h_2} < 4$ TeV.

New physics contributions $\Delta a_\mu^{\rm NP}$ to the muon anomalous magnetic moment are given at one-loop order by the Feynman diagrams depicted in Fig. 3.3. Since the couplings of a new scalar h_2 to the SM fermions are suppressed by a factor of $\sin\alpha_h$, which we find to be always smaller than 0.08 as can be seen in the bottom panel of Fig. 3.4, the right diagram in Fig. 3.3, which scales as $\Delta a_\mu^{h_2} \propto \frac{m_\mu^2}{m_{h_2}^2}\left(y_\mu \sin\alpha_h\right)^2$ with $\sin^2\alpha_h < 0.0064$ and $y_\mu = Y_e^{22}$, provides sub-leading contributions to Δa_μ. Furthermore, as we show in the top-left panel of Fig. 3.4 the new scalar boson mass, which we have found to satisfy $m_{h_2} \gtrsim 380$ GeV, is not light enough to compensate the smallness of the scalar mixing angle. Conversely, and recalling that all fermions in the B-L-SM transform non-trivially under $\mathrm{U}(1)_{\mathrm{B-L}}$, the new Z' boson can have sizeable couplings to fermions via gauge interactions proportional to $g_{\mathrm{B-L}}$. Therefore, the left diagram in Fig. 3.3 provides the leading contribution to the $(g-2)_\mu$ in the model under consideration. In particular, $\Delta a_\mu^{Z'}$ is given by [66]

$$\Delta a_\mu^{Z'} = \frac{1}{12\pi^2}\frac{m_\mu^2}{m_{Z'}^2}\left(3 g_{\rm L}^{\mu\mu Z'} g_{\rm R}^{\mu\mu Z'} - {g_{\rm L}^{\mu\mu Z'}}^2 - {g_{\rm R}^{\mu\mu Z'}}^2\right) \tag{3.35}$$

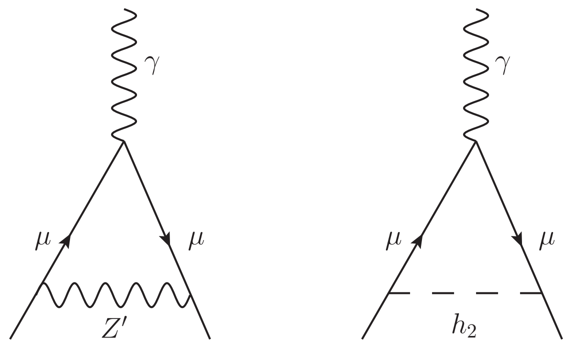

Figure 3.3: One-loop diagrams contributing to $\Delta a_\mu^{\rm NP}$ in the B-L-SM.

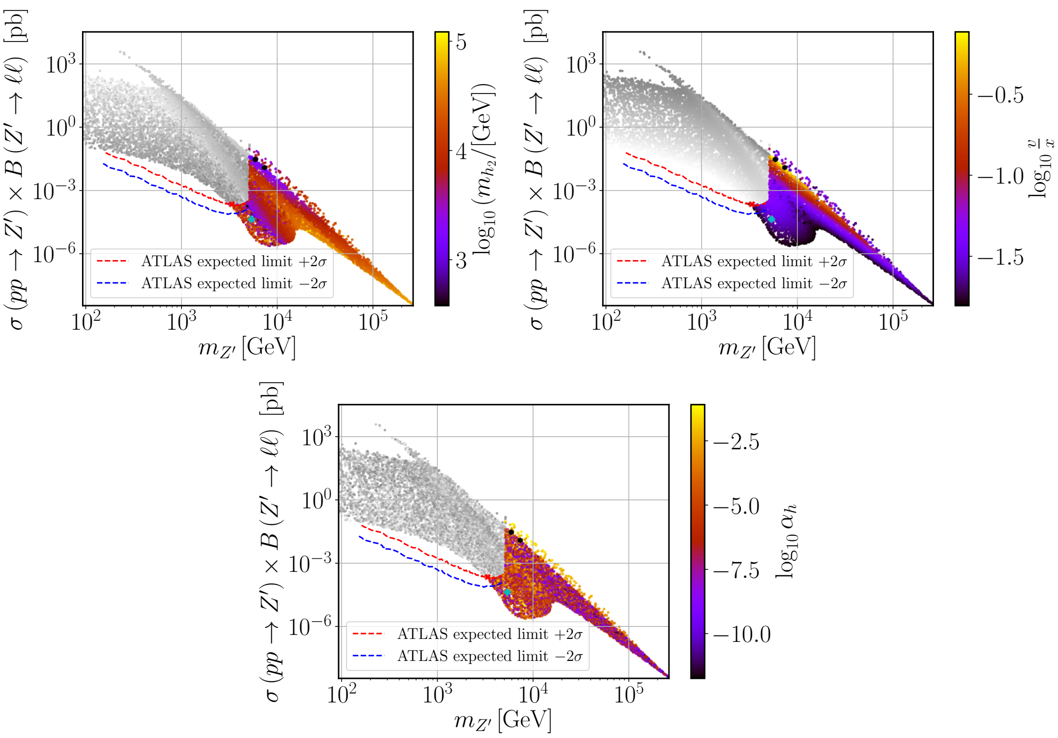

Figure 3.4: Scatter plots showing the Z' Drell-Yan production cross section times the decay branching ratio into a pair of electrons and muons in terms of the $m_{Z'}$ boson mass. The colour gradation represents the new scalar mass (top-left), the ratio between the EW- and $\mathrm{U}(1)_{\mathrm{B-L}}$-breaking VEVs (top-right) and the scalar mixing angle (bottom). The grey points are excluded by direct Z' searches at the LHC. The four benchmark points in Tab. 3.4 are represented by the black dots (last two rows), cyan diamond (first row) and red cross (second row).

---

where the left- and right-chiral projections of the charged lepton couplings to the Z' boson, $g_{\rm L}^{\ell\ell Z'}$ and $g_{\rm R}^{\ell\ell Z'}$, respectively, can be approximated as follows

$$\begin{aligned} g_{\rm L}^{\ell\ell Z'} &\simeq g_{\rm B-L} + \tfrac{1}{32}\left(\tfrac{v}{x}\right)^2 \tfrac{g_{\rm YB}}{g_{\rm B-L}}\left[g_{\rm Y}^2 - g^2 + 2g_{\rm Y}g_{\rm YB}\right]\,, \\ g_{\rm R}^{\ell\ell Z'} &\simeq g_{\rm B-L} + \tfrac{1}{16}\left(\tfrac{v}{x}\right)^2 \tfrac{g_{\rm YB}}{g_{\rm B-L}}\left[g_{\rm Y}^2 + g_{\rm Y}g_{\rm YB}\right]\,, \end{aligned} \tag{3.36}$$

to the second order in v/x-expansion. If $v/x \ll 1$, corresponding to the darker shades of the color scale in the top-right panel of Fig. 3.4, we can further approximate

$$g_{\mathrm{L}}^{\ell\ell Z'} \simeq g_{\mathrm{R}}^{\ell\ell Z'} \simeq g_{\text{B-L}}\,, \tag{3.37}$$

such that the muon anomalous magnetic moment gets significantly simplified to

$$\Delta a_{\mu}^{Z'} \simeq \frac{g_{\text{B-L}}^{2}}{12\pi^{2}}\frac{m_{\mu}^{2}}{m_{Z'}^{2}}\,. \tag{3.38}$$

Similarly, for the yellow band, which corresponds to the region where $\Delta a_{\mu}^{\mathrm{NP}}$ is maximized (see top-left panel of Fig. 3.2), a large value of the $\mathrm{U}(1)_{\mathrm{B-L}}$ gauge coupling also allows one to simplify Eq. (3.35) reducing it to the form of Eq. (3.38). This is in fact what we have observed and, for the yellow band region, we see in the bottom panel of Fig. 3.5 that $g_{\text{B-L}} \simeq 3$. A sizeable value of $g_{\text{B-L}}$ is indeed what is contributing to the enhancement of $\Delta a_{\mu}^{\mathrm{NP}}$, in particular, for the red region in both panels of Fig. 3.2. We show in the third and fourth lines of Tab. 3.4 the two benchmark points that better reproduce the muon anomalous magnetic moment represented by two black dots in Figs. 3.2, 3.4 to 3.6.

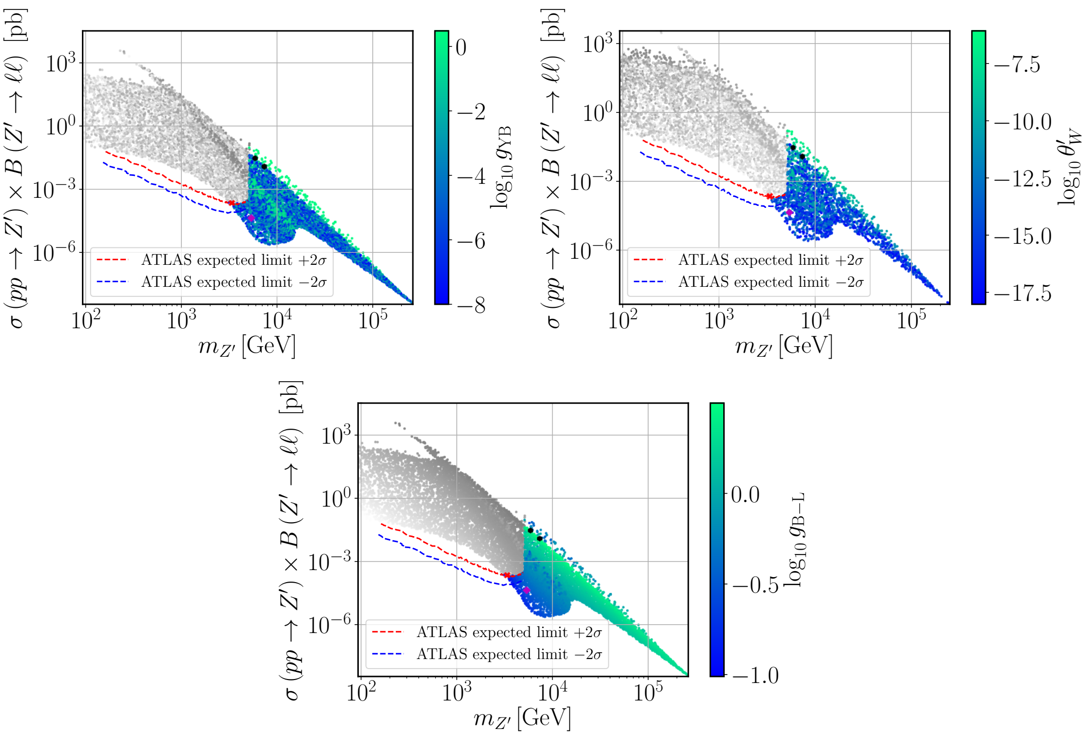

Figure 3.5: The same as in Fig. 3.4 but with the colour scale representing the gauge-mixing parameters g_{YB} (top-left) and θ'_W (top-right), and the $\mathrm{U}(1)_{\mathrm{B-L}}$ gauge coupling (bottom).

In fact, a close inspection of Fig. 3.2 (left panel) and Fig. 3.4 (top-right panel) reveals an almost one-to-one correspondence between the colour shades. This suggests that $\Delta a_{\mu}^{Z'}$ must somehow be related to the VEV ratio v/x. To understand this behaviour, let us also look to Fig. 3.5 (top-right panel) where we see that the kinetic-mixing gauge coupling g_{YB} is typically very small apart from two green bands where it can become of order $\mathcal{O}(1)$. Interestingly, whenever g_{YB} becomes sizeable, $v/x \ll 1$ is realised, which means that Eq. (3.26) is indeed a good approximation as was argued above. It is then possible to eliminate $g_{\text{B-L}}$ from Eq. (3.38) and rewrite it as

$$\Delta a_{\mu}^{Z'} \simeq \frac{y_{\mu}^{2}}{96\pi^{2}}\left(\frac{v}{x}\right)^{2}, \tag{3.39}$$

which explains the observed correlation between both Fig. 3.2 (left panel) and Fig. 3.4 (top-right panel) and, for instance, the thin red stripe of points compatible with a full description of the muon $(g-2)_\mu/2$ anomaly. Note that this simple and illuminating relation becomes valid as a consequence of the heavy Z' mass regime, in combination with the smallness of the θ'_W mixing angle required by LEP constraints. Indeed, while we have not imposed any strong restriction on the input parameters of our scan (see Tab. 3.3), Eq. (3.22) necessarily implies that both $g_{\rm YB}$ and v/x cannot be simultaneously sizeable in agreement with what is seen in Fig. 3.5 (top-left panel) and Fig. 3.4 (top-right panel). The values of θ'_W obtained in our scan are shown in the top-right panel of Fig. 3.5.

For completeness, we show in Fig. 3.6 the physical couplings of Z' to muons (top panels) and to $W^\pm$ bosons (bottom panel). Note that, for the considered scenarios, the latter can be written

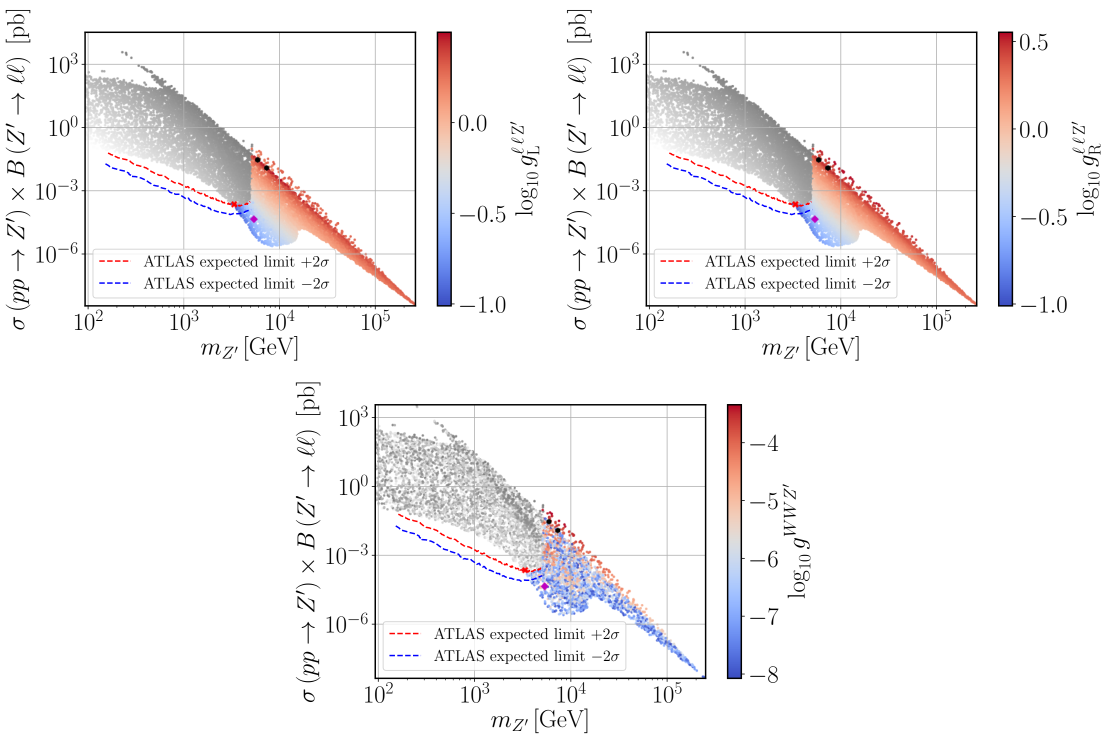

Figure 3.6: The same as in Fig. 3.4 but with the colour scale representing the coupling of leptons to the Z' (top panels) and the coupling of W bosons to Z'.

as

$$g^{WWZ'} \simeq \frac{1}{16}\frac{g_{\rm YB}}{g_{\rm B\text{-}L}}\left(\frac{v}{x}\right)^2 \,. \tag{3.40}$$

While both $g_{\rm B\text{-}L}$ and the ratio v/x provide a smooth continuous contribution in the $\sigma B - m_{Z'}$ projection of the parameter space, the observed blurry region in $g^{WWZ'}$ is correlated with the one in the top-left panel of Fig. 3.5 as expected from Eq. (3.40). On the other hand, the couplings to leptons $g_{\rm L,R}^{\ell\ell Z'}$ exhibit a strong correlation with $g_{\rm B\text{-}L}$ in Fig. 3.5, in agreement with our discussion above and with Eq. (3.37).

Barr-Zee type contributions

To conclude our analysis, one should note that the two-loop Barr-Zee type diagrams [67] are always sub-dominant in our case. To see this, let us consider the four diagrams shown in Fig. 3.7. The same reason that suppresses the one-loop h_2 contribution in Fig. 3.3 is also responsible for the suppression of both the top-right and bottom-right diagrams in Fig. 3.7 (for details see

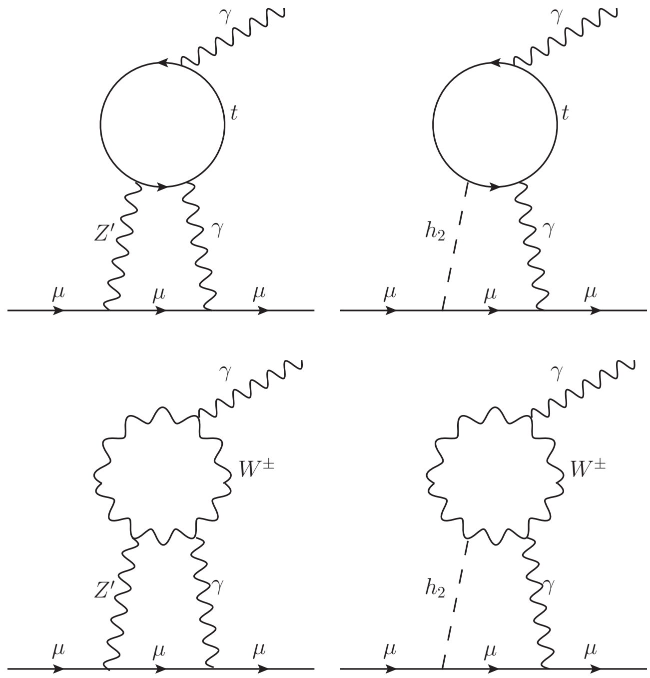

Figure 3.7: Barr-Zee type two-loop diagrams contributing to Δa_μ.

e.g. Ref. [68]). Recall that the coupling of h_2 to the SM particles is proportional to the scalar mixing angle α_h, which is always small (or very small) as we can see in Fig. 3.4. An analogous effect is present in the diagram involving a W-loop, where a vertex proportional to $g^{WWZ'}$ suppresses such a contribution. The only diagram that might play a sizeable role is the top-left one where the couplings of Z' to both muons and top quarks are not negligible.

Let us then estimate the size of the first diagram in Fig. 3.7. This type of diagrams were already calculated in Ref. [69] but for the case of a SM Z-boson. Since the same topology holds for the considered case of B-L-SM too, if we trade Z by the new Z' boson, the contribution to the muon $(g-2)_\mu$ anomaly can be rewritten as

$$\Delta a_\mu^{\gamma Z'} = -\frac{g^2 g_{\text{B-L}}^2 m_\mu^2 \tan^2\theta_W}{1536\pi^4}\left(g_{\text{L}}^{ttZ'} - g_{\text{R}}^{ttZ'}\right)\text{T}_7\left(m_{Z'}^2, m_t^2, m_t^2\right)\,, \tag{3.41}$$

where $g_{\text{L,R}}^{ttZ'}$, calculated in `SARAH`, are the left- and right-chirality projections of the Z' coupling to top-quarks, given by

$$\begin{aligned} g_{\text{L}}^{ttZ'} &= -\frac{g_{\text{B-L}}}{3}\cos\theta'_W + \frac{g}{2}\cos\theta_W\sin\theta'_W - \frac{g_{\text{Y}}}{6}\sin\theta_W\sin\theta'_W - \frac{g_{\text{YB}}}{3}\sin\theta_W\sin\theta'_W\,,\\ g_{\text{R}}^{ttZ'} &= -\frac{g_{\text{B-L}}}{3}\cos\theta'_W - \frac{2g_{\text{Y}}}{3}\sin\theta_W\sin\theta'_W - \frac{g_{\text{YB}}}{3}\sin\theta_W\sin\theta'_W\,. \end{aligned} \tag{3.42}$$

The loop integral $\text{T}_7\left(m_{Z'}^2, m_t^2, m_t^2\right)$ was determined in Ref. [69] and, in the limit $m_{Z'} \gg m_t$, as we show in Eq. (6.11), it gets simplified to

$$\text{T}_7\left(m_{Z'}^2, m_t^2, m_t^2\right) \simeq \frac{2}{m_{Z'}^2}\,, \tag{3.43}$$

up to a small truncation error (see Appendix 6.1 for details). For the parameter space region under consideration the difference $g_{\text{L}}^{ttZ'} - g_{\text{R}}^{ttZ'}$ can be cast in a simplified form as follows

$$\left(g_{\text{L}}^{ttZ'} - g_{\text{R}}^{ttZ'}\right) \simeq \frac{\left(g^2 + g_{\text{Y}}^2\right) g_{\text{YB}}}{32 g_{\text{B-L}}}\left(\frac{v}{x}\right)^2\,. \tag{3.44}$$

Using this result and the approximate value of the loop factor, we can calculate the ratio between the two- and one-loop contributions to the muon $(g-2)_\mu$,

$$\frac{\Delta a_\mu^{\gamma Z'}}{\Delta a_\mu^{Z'}} \simeq -\frac{g^2 g_{\mathrm{Y}^2}}{2048\pi^2}\frac{g_{\mathrm{YB}}}{g_{\mathrm{B\text{-}L}}}\left(\frac{v}{x}\right)^2 \ll 1\,, \tag{3.45}$$

which shows that $\Delta a_\mu^{\gamma Z'}$ does indeed play a subdominant role in our analysis and can be safely neglected.

3.3 The B-L-SM Conclusions

In this chapter, we have confronted the model with the most recent experimental bounds from the direct Z' boson and next-to-lightest Higgs state searches at the LHC. Simultaneously, we have analysed the prospects of the B-L-SM for a consistent explanation of the observed anomaly in the muon anomalous magnetic moment $(g-2)_\mu$. Done through exploring B-L-SM potential for the observed $(g-2)_\mu$ anomaly in the regions of the model parameter space that are consistent with direct searches and electroweak precision observables.

As one of the main results of our analysis, we have found phenomenologically consistent model parameter space regions that simultaneously fit the exclusion limits from direct Z' searches and can explain the muon $(g-2)_\mu$ anomaly. We have distinguished four benchmark points for future phenomenological exploration at experiments, the first one with the lightest allowed Z' ($m_{Z'} > 3.1$ TeV), the second with the lightest additional scalar boson ($m_{h_2} > 400$ GeV), and the other two points that reproduce the muon $(g-2)_\mu$ anomaly within 1σ uncertainty range. Besides, we have studied the correlations of the Z' production cross section times the branching ratio into a pair of light leptons versus the physical parameters of the model. In particular, we have found that the muon $(g-2)_\mu$ observable dominated by Z' loop contributions lies within the phenomenologically viable parameter space domain. For completeness, we have also estimated the dominant contribution from the Barr-Zee type two-loop corrections and found a relatively small effect.

Chapter 4

Proper 3HDM

4.1 Introduction

Now having finished the analysis of a simple unitary extension, it is time to present a more complex model. The goal of this chapter will be to first introduce all the required theoretical background to analysis a three Higgs Doublet Model (3HDM), specifically a minimal BGL (Branco-Grimus-Lavoura) like 3HDM. Then moving to present a phenomenological simulation similar as before, as to observe the state of the art in the 3HDM. This simulation used a newer version of the previously discussed mechanism with the addition of a flavour calculation package based on python3 entitled "flavio" citation needed

This 3HDM model is part of a larger family of multiple Higgs Doublet Models, or NHDMs, the first iteration of which was the 2HDM model. As before mentioned, one of the simplest ways to expand the SM is to add elements to it's scalar sectors. In these types of models, in parallel with the standard SM Higgs doublet some additional replicas of that same doublet are introduced. In the 3HDM these form a sort of family in the scalar sector in analogy to the fermion sector. This idea is far from original and was first discussed by Weinberg in, [70].

These additional Higgs doublet are valid given they do not alter the tree-level electroweak ρ parameter as long the condition that the sum of the doublet VEVs are equal the value for the electroweak VEV in case of the SM citation needed. Although this value can vary by 20% citation needed there are many reason as to impose this condition. This is the part of a wider *alignment limit* condition that will be discussed further on, in depth. True?

The basis for our BGL like treatment of a 3HDM will be the inclusion of a flavour symmetry, as to attempt to constrain the flavour observables. In particular the addition of a $\mathrm{U}(1)\times\mathrm{Z}_2$ symmetry. This symmetry constrains the terms that can appear in the flavour sector of the Lagrangian resulting in very specific structures (or textures) of the Yukawa couplings. We will show how this structure combined with the off diagonal terms of the CKM matrix lead to controlled values for FCNCs. Then showing that light scalars are still within the reach of future collider experiments in our model's framework while having FCNCs concurrent with observations and respecting many more theoretical and experimental bounds, such as in our previous analysis.

4.1.1 Context, the case of the BGL-2HDM

The first model that attempted to perform a doublet based extension was the Two Higgs Doublet Model (2HDM) proposed by T.D. Lee [71]. His work motivated by the search for a spontaneous breaking of the CP symmetry.

A great deal of interest was invested in 2HDMs, given their possible dark matter candidates large particle spectrum, including charged and additional neutral scalars. However, take in consideration that in most 2HDM structures the possibility of tree-level scalar mediated FCNCs emerged. A analysis of their origin led to disturbing conclusions, given the fermions now have their mass generated by several Yukawa matrices their simultaneous diagonalization wasn't guaranteed. These tree-level FCNCs are, in most cases, in direct opposition to experimental results, as discussed in Chapter 1. In fact, Consulting the literature, as in, [72], we see that this forces the extra scalars in the 2HDM case to have masses above 1 TeV. These heavy scalars although a possibility given current observations, are far from ideal, since there is no indication such heavy scalars exist nor do they provide us with interesting physics. There-for several mechanisms have been proposed to deal with suppress these tree-level FCNCs as to allow for richer physics. First, in, [73, 74, 75], it is proposed a framework in which we have the balancing of CP-odd and CP-even contribution to FCNCs, however, this would requires some fine-tuning, making it very unappealing. Another possibility is to assume alignment between different Yukawa matrices such that no FCNCs are present, see [76, 77, 78] for more information. Finally we could also use the approach presented in the BGL version of the 2HDM [79, 80], here the authors impose a flavour-violating symmetry naturally keeping the FCNCs under control trough the CKM matrix. The phenomenology of the model has been studied quite thoroughly in previous works, see Refs. [81, 82], and it remains a possible scenario for BSM physics. Inspired by this BGL model our studies will try to reproduce a similar mechanism on a 3HDM Model.

4.2 The formulation of a BGL-like 3HDM

Challenging the 2HDM BGL paradigm can be motivated by some phenomenological comparison of the 3HDM to the 2HDM model more than just by the "naturalist" family argument. For example, vacuum stability in the 2HDM model can only accommodate one instance of spontaneous CP or charge symmetry breaking [83, 84, 85]. However in Multiple Higgs Doublets models (NHDMs), such as the 3HDM, charge breaking minima were found to be stable while at the same time coexisting with charge-preserving ones, for more information see, [86]. Also, for the 2HDM a full list of all possible incorporations of symmetries consistent with $\mathrm{SU}(2)\times\mathrm{U}(1)$ has been achieved [87, 88], while for the 3HDM no work has thus far been completed, see, [89, 90]. Moreover generic unitarity constraints have been found for the 2HDM [91] but not for 3HDMs. Not to mention these models provide a richer playground for experimental detection and testing than the 2HDM give it's extended scalar sector.

4.2.1 Fields and the Additional $\mathrm{U}(1)\times\mathbb{Z}_2$ Symmetry

In a sense this model is extension of the SM as it still includes all the same fields with same charges under the $\mathcal{G}_{SM}$ as we saw in chapter 1. Making the particle content of the model is pretty similar to the SM. Having the same gauge fields and the following fermion and scalar fields,

$$\begin{aligned}
Q_{L_i} &= \begin{pmatrix} u_{L_i} \\ d_{L_i} \end{pmatrix} \quad , \quad \Psi_{L_i} = \begin{pmatrix} \nu_{L_i} \\ e_{L_i} \end{pmatrix} \quad , \\
& u_{R_i} \quad , \quad d_{R_i} \quad , \quad e_{R_i} \quad i = \{1,2,3\} \quad , \\
\phi_k &= \begin{pmatrix} W_k^{\pm} + i\, W_k^{\mp} \\ \frac{1}{\sqrt{2}}\left(v_k + h_k + iZ_k\right) \end{pmatrix} \quad , \quad k = \{1,2,3\} \quad .
\end{aligned} \tag{4.1}$$

where Q_{L_i} , ϕ_k , Ψ_{L_i} and u_{R_i}, d_{R_i}, e_{R_i} are $\mathrm{SU}(2)_L$ doublets and singlets of the i-th and k-th generation, respectively. However the new charges under $\mathrm{U}(1)\times\mathbb{Z}_2$ must be specified. They show themselves in the transformation these fields can perform,

$$\begin{array}{ll}
\mathrm{U}(1): & \mathbb{Z}_2: \\
\quad Q_{L_3} \to e^{i\alpha} Q_{L_3} & \quad Q_{L_3} \to -Q_{L_3} \\
\quad u_{R_3} \to e^{2i\alpha} u_{R_3} & \quad u_{R_3} \to -u_{R_3} \\
\quad \phi_1 \to e^{i\alpha} \phi_1 & \quad \phi_1 \to -\phi_1 \\
\quad \Psi_{L_1} \to e^{i\alpha} \Psi_{L_1} & \quad \Psi_{L_1} \to -\Psi_{L_1} \\
\quad \phi_3 \to e^{i\alpha} \phi_3 & \quad \phi_3 \to -\phi_3
\end{array} \tag{4.2}$$

All remaining fields not shown in Eq. 4.2 remain unchanged under transformations of the $U(1) \times \mathbb{Z}_2$ global symmetry (one scalar field and two fermion generations). This symmetry will have to be softly broken as to avoid the appearance of a massless Goldstone state.

Note there is no right handed neutrino fields in this model making it so that no neutrino mass terms appear. check with morais

4.2.2 Introducing The Scalar Sector

Let us then start our proper introduction to the workings of the model by presenting the scalar sector where the new spin-0 SU(2) doublets, ϕ_i, $i = \{1, 2, 3\}$ reside. Note the scalar potential to be CP-invariant, this means,

$$\phi_1 = \phi_1^* \quad , \quad \phi_2 = \phi_2^* \quad , \quad \phi_3 = \phi_3^* \tag{4.3}$$

The generic scalar potential that follows all these transformations is extensively written in,

$$\begin{aligned} V(\phi_i) = & - \mu_1^2 \left(\phi_1^\dagger \phi_1\right) - \mu_2^2 \left(\phi_2^\dagger \phi_2\right) - \mu_3^2 \left(\phi_3^\dagger \phi_3\right) \\ & \left[-\mu_{12}^2 \left(\phi_1^\dagger \phi_2\right) - \mu_{23}^2 \left(\phi_2^\dagger \phi_3\right) - \mu_{13}^2 \left(\phi_1^\dagger \phi_3\right) + h.c.\right] \\ & + \lambda_1 \left(\phi_1^\dagger \phi_1\right) + \lambda_2 \left(\phi_2^\dagger \phi_2\right) + \lambda_3 \left(\phi_3^\dagger \phi_3\right) \\ & + \lambda_4 \left(\phi_1^\dagger \phi_1\right)\left(\phi_2^\dagger \phi_2\right) + \lambda_5 \left(\phi_1^\dagger \phi_1\right)\left(\phi_3^\dagger \phi_3\right) + \lambda_6 \left(\phi_2^\dagger \phi_2\right)\left(\phi_3^\dagger \phi_3\right) \\ & + \lambda_7 \left(\phi_1^\dagger \phi_2\right)\left(\phi_1^\dagger \phi_2\right) + \lambda_8 \left(\phi_1^\dagger \phi_3\right)\left(\phi_3^\dagger \phi_1\right) + \lambda_9 \left(\phi_2^\dagger \phi_3\right)\left(\phi_3^\dagger \phi_2\right) \\ & + \lambda_{10} \left\{ \left(\phi_1^\dagger \phi_3\right)^2 + \text{h.c.} \right\} \end{aligned} \tag{4.4}$$

Due to the $\mathcal{CP}$ symmetry imposed on this potential all parameters, $(\lambda_i, i = \{1, ..., 10\})$, here are real. The parameter μ_{23}, is necessarily added as to impede the formation of a massless axion. However the most generic version of this soft breaking is given by the second line. After the process of SBB, all Higgs doublets take a VEV shape similar to that of the SM Higgs, written as,

$$\phi_k = \begin{pmatrix} W_k^\pm + i\, W_k^\mp \\ \frac{1}{\sqrt{2}} \left(v_k + h_k + i Z_k\right) \end{pmatrix} \rightarrow \langle \phi_k \rangle = \begin{pmatrix} 0 \\ \frac{v_k}{\sqrt{2}} \end{pmatrix} \quad , \quad k = \{1, 2, 3\} \tag{4.5}$$

Here we see the charged portion of the field, $W_k^\pm$, the CP-odd portion, Z_k, and finally the CP-even, h_k.

Recall that, for the given scalar potential V as seen in Eq 4.4 to have a stable vacuum it needs to satisfy *boundness from below* conditions. As before this will ensure that there is indeed an absolute minimum of energy. To solve these one must write the derivates of the potential with respect to the fields and then observe their values once the process of SBB occurs, this process yields the following equations,

$$\begin{aligned} \frac{\partial V}{\partial \phi_1} = & \frac{1}{2} v_1 \left(\left(2\lambda_{10} + \lambda_5 + \lambda_8\right) v_3 + 2\left(\lambda_1 v_1 + \mu_1^2\right) + \left(\lambda_4 + \lambda_7\right) \right) \\ \frac{\partial V}{\partial \phi_2} = & \frac{1}{2} v_2 \left(2\left(\lambda_2 v_2^2 + \mu_2^2\right) + \left(\lambda_4 + \lambda_7\right) v_1^2 + \left(\lambda_9 + \lambda_6\right) v_3^2 \right) + \mu_{23} v_3 \\ \frac{\partial V}{\partial \phi_3} = & \frac{1}{2} \left(\left(2\lambda_{10} + \lambda_5 + \lambda_8\right) v_1^2 + 2\mu_3^2 + \left(\lambda_6 + \lambda_9\right) v_2^2 \right) v_3 + \lambda_3 v_3^3 + \mu_{23}^2 v_2 \end{aligned} \tag{4.6}$$

By requiring that the derivatives of the potential vanish for some value of the CP-even fields ϕ_i , one arrives at the so-called tadpole equations of the model. And trough the tadpole equations in

Eq. 4.6, we could express the quadratic terms μ_1, μ_2 and μ_3 as follows,

$$\begin{aligned}
\mu_1^2 &= \lambda_1 v_1^2 + \frac{1}{2}\left(\lambda_4+\lambda_7\right)v_2^2 + \frac{1}{2}\left(\lambda_5+\lambda_8+2\lambda_{10}\right)v_2^2 \\
\mu_2^2 &= \lambda_2 v_2^2 + \frac{1}{2}\left(\lambda_4+\lambda_7\right)v_1^2 + \frac{1}{2}\left(\lambda_6+\lambda_9\right)v_3^2 + \frac{v_3}{v_2}\mu_{23}^2 \\
\mu_3^2 &= \lambda_3 v_3^2 + \frac{1}{2}\left(\lambda_6+\lambda_9\right)v_2^2 + \frac{1}{2}\left(\lambda_5+\lambda_8+2\lambda_{10}\right)v_1^2 + \frac{v_2}{v_3}\mu_{23}^2
\end{aligned} \tag{4.7}$$

The Alignment Limit

Let us first consider the Gauge portion of the 3HDM Lagrangian. After the Higgs Doublets shift to their VEVs we have the following mass terms,

$$\mathcal{L}_{\text{gauge}} \supset \frac{1}{4}\left(v_1^2+v_2^2+v_3^2\right)g^2 W_\mu^+ W^{-\,\mu} + \frac{1}{8}\left(v_1^2+v_2^2+v_3^2\right)\left(g'^{\,2}+g^2\right)Z_\mu Z^\mu \tag{4.8}$$

where we can clearly see that to reproduce the correct Gauge boson masses we must ensure that,

$$\sum_{k=1}^{3} v_k^2 \approx 246^2\text{GeV} \quad . \tag{4.9}$$

This is a very important condition as it will reflect what range of values are available for our Higgs Doublets to take. It also enables us to perform the following parametrization,

$$v_1 = v\cos(\psi_1)\cos(\psi_2) \quad , \quad v_2 = v\sin(\psi_1)\cos(\psi_2) \quad , \quad v_3 = v\sin(\psi_2) \tag{4.10}$$

where now the VEVs are written as a combination of a magnitude $v = \sqrt{v_1^2+v_2^2+v_3^2}$ and two mixing angles ψ_1 and ψ_2.

Through this parametrization we can write the orthogonal mixing matrix,

$$\mathcal{O} = \begin{pmatrix} \cos(\psi_1)\cos(\psi_2) & \cos(\psi_2)\sin(\psi_1) & \sin(\psi_2) \\ -\sin(\psi_1) & \cos(\psi_1) & 0 \\ -\cos(\psi_1)\sin(\psi_2) & \sin(\psi_1)\sin(\psi_2) & \cos(\psi_2) \end{pmatrix} \tag{4.11}$$

This matrix is going to form a fundamental part of our diagonalization of massive scalar states. This matrix will be responsible for giving us a intermediate basis, specifically between the gauge and mass basis, that will call the Higgs basis.

Asides from ensure the proper Gauge boson masses we must also account for the proper Gauge-Higgs interactions. We observe Lagrangian terms of the form,

$$\frac{g^2 v}{2} W_\mu^+ W^{\mu\,-}\left(\frac{1}{v}\sum_{k=1}^{3} h_k v_k\right) \tag{4.12}$$

We clearly see this to be CP-even Higgs states interacting with the $W^\pm$ bosons, so apriori we must ensure that this represents a physical state relating to the SM Higgs Boson as,

$$h_1 = \left(\frac{1}{v}\sum_{k=1}^{3} h_k v_k\right) \tag{4.13}$$

Otherwise different tree-level couplings to the gauge bosons would show themselves.

This is the so called Higgs alignment limit. Where we force a eigenstate of the Gauge base to serve as the observed Higgs Boson, leading to a complete superposition of both physical and gauge eigenstates. For a more detailed description of the process see Ref. [92].

4.2.3 The CP-odd portion of the scalar sector

We can now turn our attention to the physical scalar spectrum of the model. This potential is explicitly CP invariant given all parameters are real (VEVs, couplings and quadratic masses). In fact in this model we expect to find no more sources of CP-violation than in the SM.

Pseudoscalar Eigenstates

The CP-odd portion of the scalar sector (related to the z_k degrees of freedom) contains quadratic terms after the process of SBB. These are easily extracted from the scalar potential in the form,

$$V_{\text{shifted}} \supset \begin{pmatrix} z_1 & z_2 & z_3 \end{pmatrix} \frac{M_P^2}{2} \begin{pmatrix} z_1 \\ z_2 \\ z_3 \end{pmatrix} \tag{4.14}$$

where M_P^2 is the 3×3 pseudoscalar mass matrix in a non diagonal form, i.e. in a unphysical basis. It can however be expressed in a block diagonalized trough the rotation matrix we introduced in Eq. 4.11, as,

$$B_P^2 = \mathcal{O} M_P^2 \mathcal{O}^T = \begin{pmatrix} 0 & 0 & 0 \\ 0 & \left(B_P^2\right)_{22} & \left(B_P^2\right)_{23} \\ 0 & \left(B_P^2\right)_{32} & \left(B_P^2\right)_{33} \end{pmatrix} \tag{4.15}$$

The line and column of zeroes in this matrix tells us that it has a zero eigenvalue. This eigenstate will provide a Goldstone, this is clearly the Goldstone that will become the longitudinal polarization of the Z. The remaining elements of the B_P^2 matrix are given by,

$$\begin{aligned} \left(B_P^2\right)_{22} =& \frac{v_3\left(-2v_2^3 v_3 \lambda_1 0 + v_1^2 \mu_{23}^2\right)}{v_2\left(v_1^2+v_2^2\right)} \\ \left(B_P^2\right)_{32} = \left(B_P^2\right)_{23} =& \frac{v_1 v\left(2v_2 v_3 \lambda_{10} + \mu_{23}^2\right)}{v_2^2+v_1^2} \\ \left(B_P^2\right)_{33} =& \frac{v^2\left(2v_1^2 v_3 \lambda_{10} - v_2 \mu_{23}^2\right)}{\left(v_2^2+v_1^2\right) v_3} \end{aligned} \tag{4.16}$$

From the above equations we notice that, apart from the three VEVs, only two parameters, λ_{10} and μ_{23}, enter in the pseudoscalar mass eigensystem. Given this fact, we can introduce a final orthogonal matrix,

$$\mathcal{O}_{\gamma_1} = \begin{pmatrix} 1 & 0 & 0 \\ 0 & \cos(\gamma_1) & -\sin(\gamma_) \\ 0 & \sin(\gamma_1) & \cos(\gamma_1) \end{pmatrix} \tag{4.17}$$

Making the mass eigenstates in the mass basis to be,

$$\mathcal{O}_{\gamma_1} \left(B_P\right)^2 \mathcal{O}_{\gamma_1}^T = \begin{pmatrix} 0 & 0 & 0 \\ 0 & M_{A_1} & 0 \\ 0 & 0 & M_{A_2} \end{pmatrix} \tag{4.18}$$

Here we have the final massive states, A_1 and A_2. Furthermore, through the conditions,

$$\begin{aligned} \mathrm{Tr}(B_C^2) &= m_{A_1} + m_{A_2} \\ \mathrm{Det}(B_P^2) &= m_{A_1} m_{A_2} \end{aligned} \tag{4.19}$$

We can express the mass of these pseudoscalars as a parametrization of, λ_{10}, v, and mixing angles ψ_1 and ψ_2.

$$\begin{aligned} m_{A_1} &= -2\lambda_{10}v^2\left(1-\sin(\psi_1)^2\cos(\psi_2)^2\right) \\ m_{A_2} &= \frac{\mu_2 3}{\sin(\psi_1)\sin(\psi_2)\cos(\psi_2)}\left(1-\cos(\psi_1)^2\cos(\psi_2)^2\right) \end{aligned} \tag{4.20}$$

Charged Scalar Eigenstates

Through a similar process, we can endeavour to isolate the quadratic terms relating to the charged degrees of freedom. These fields produce a similar structure to the mass matrix of the pseudoscalar fields.

$$B_C^2 = \mathcal{O}M_C^2\mathcal{O}^T = \begin{pmatrix} 0 & 0 & 0 \\ 0 & \left(B_C^2\right)_{22} & \left(B_C^2\right)_{23} \\ 0 & \left(B_C^2\right)_{32} & \left(B_C^2\right)_{33} \end{pmatrix} \tag{4.21}$$

Here we observe again that a line and column of zeros ensures that we have a Goldstone boson for the $W^\pm$. In the same fashion as before we define the terms of Eq.4.21,

$$\begin{aligned} \left(B_C^2\right)_{22} &= -\frac{1}{2v_2(v_1^2+v_2^2)}\Big[v_2^5\lambda_7 + v_2^3\left(2v_1^2\lambda_7 + v_3^2\left(2\lambda_{10}+\lambda_8\right)\right) \\ &\qquad + v_2\left(v_1^4\lambda_7 + v_1^2v_3^2\lambda_9\right) - 2v_1^2v_3\mu_{23}^2\Big] \\ \left(B_C^2\right)_{32} &= \frac{v_1 v}{2(v_1^2+v_2^2)}\left[v_2v_3\left(2\lambda_{10}+\lambda_8-\lambda_9\right)+2\mu_{23}^2\right] \\ \left(B_C^2\right)_{33} &= \frac{v^2}{2(v_1^2+v_2^2)v_3}\left[v_1^2v_3\left(2\lambda_{10}+\lambda_8\right)+v_2\left(v_2v_3\lambda_9-2\mu_{23}^2\right)\right] \end{aligned} \tag{4.22}$$

Again we need to introduce another base changing rotation matrix. This is,

$$\mathcal{O}_{\gamma_2} = \begin{pmatrix} 1 & 0 & 0 \\ 0 & \cos(\gamma_2) & -\sin(\gamma_2) \\ 0 & \sin(\gamma_2) & \cos(\gamma_2) \end{pmatrix} \tag{4.23}$$

Making the mass eigenstates in the mass basis to be,

$$\mathcal{O}_{\gamma_1}\left(B_C\right)^2\mathcal{O}_{\gamma_1}^T = \begin{pmatrix} 0 & 0 & 0 \\ 0 & M_{H_1^\pm} & 0 \\ 0 & 0 & M_{H_2^\pm} \end{pmatrix} \tag{4.24}$$

Where we see the explicit mass eigenstates of the charged scalars $H_1^\pm$ and $H_2^\pm$. Trough these matrices we can arrive at another parametrization,

$$\begin{aligned} m_{H_1^\pm}\cos^2(\gamma_2) + m_{H_2^\pm}\sin^2(\gamma_2) &= \left(B_C^2\right)_{22} \\ \cos(\gamma_2)\sin(\gamma_2)(m_{H_2^\pm}^2 - m_{H_1^\pm}^2) &= \left(B_C^2\right)_{23} \\ m_{H_1^\pm}\sin^2(\gamma_2) + m_{H_2^\pm}\cos^2(\gamma_2) &= \left(B_C^2\right)_{33} \end{aligned} \tag{4.25}$$

Here, another three parameters, λ_{7-9} of the potential can be expressed in terms of physical masses and a mixing angle.

$$\begin{aligned} \lambda_7 &= \sin(\lambda_1) \\ \lambda_8 &= \\ \lambda_9 &= \end{aligned} \tag{4.26}$$

4.2.4 The CP-even portion of the scalar sector

Following the same procedure as we did for the CP-odd portion we begin by approaching the quadratic portion of the scalar fields in the potential,

$$V \supset \begin{pmatrix} h_1 & h_2 & h_3 \end{pmatrix} \frac{M_S^2}{2} \begin{pmatrix} h_1 \\ h_2 \\ h_3 \end{pmatrix} \tag{4.27}$$

where M_S^2 is a 3×3 symmetric matrix. The elements of this matrix are given by,

$$M_S^2 = \begin{pmatrix} 2v_1^2\lambda_1 & v_1 v_2 \left(\lambda_4 + \lambda_7\right) & v_1 v_3 \left(\lambda_{10} + \lambda_5 + \lambda_8\right) \\ 0 & 2v_2^2\lambda_2 + \frac{v_3\mu_{23}^2}{v_2} & v_2 v_3 \left(\lambda_6 + \lambda_9\right) - \mu_{23}^2 \\ 0 & 0 & 2v_3^2\lambda_3 + \frac{v_2\mu_{23}^2}{v_3} \end{pmatrix} \tag{4.28}$$

This matrix has to be diagonalized to reach the massive eigenstates. Moving to the mass basis, h, H_1 and H_2, we use a complementary orgtogonal rotation, $\mathcal{O}_\alpha$,

$$\begin{pmatrix} h \\ H_1 \\ H_2 \end{pmatrix} = \mathcal{O}_\alpha \mathcal{O} \begin{pmatrix} h_1 \\ h_2 \\ h_3 \end{pmatrix} \tag{4.29}$$

Here $\mathcal{O}_\alpha$ can be parametrized as,

$$\mathcal{O}_\alpha = R_1 \cdot R_2 \cdot R_3 \quad , \tag{4.30}$$

with,

$$R_1 = \begin{pmatrix} \cos(\alpha_1) & \sin(\alpha_1) & 0 \\ -\sin(\alpha_1) & \cos(\alpha_1) & 0 \\ 0 & 0 & 1 \end{pmatrix} \quad , \quad R_2 = \begin{pmatrix} \cos(\alpha_2) & 0 & \sin(\alpha_2) \\ 0 & 1 & 0 \\ -\sin(\alpha_2) & 0 & \cos(\alpha_2) \end{pmatrix} \quad , \tag{4.31}$$

$$\tag{4.32}$$

$$R_3 = \begin{pmatrix} 1 & 0 & 0 \\ 0 & \cos(\alpha_3) & \sin(\alpha_3) \\ 0 & -\sin(\alpha_3) & \cos(\alpha_3) \end{pmatrix} \quad . \tag{4.33}$$

Through this $\mathcal{O}_\alpha$ we can diagonalize scalar massive eigenstates.

$$\mathcal{O}_\alpha \underbrace{\mathcal{O} M_S^2 \mathcal{O}^T}_{B_S^2} \mathcal{O}_\alpha^T \equiv \mathrm{diag}(m_h, m_{H_1}, m_{H_2}) \tag{4.34}$$

Here we can perform another inversion, allowing us to reach a parametrization of the six remaining couplings,

$$\begin{matrix} \lambda_1 \\ \lambda_2 \\ \lambda_3 \\ \lambda_4 \\ \lambda_5 \\ \lambda_6 \end{matrix} \tag{4.35}$$

To recapitulate, we can express the original fourteen real parameters of the potential in terms of physical constants. First using tadpole equations to reach μ_{11} , μ_{22} and μ_{33} in relation to the three VEVs. Secondly μ_{23} and $\lambda_1 0$, can be exchanged for m_{A_1} and m_{A_2}. Finally the remaining nine quartic couplings five physical masses (three CP-even scalars, and two charged scalars) and three mixing angles (three in the CP-even sector and one in the charged scalar sector).

In all these relations will impose the strict alignment limit condition. This translates in the lightest scalar state m_h equal to 125.09 GeV, thus making α_1 and α_2 equal to ψ_1 and ψ_2. This forces all interactions of the lightest scalar h_1 to be exactly like that of the SM, ensure it's interactions with the W and Z boson remain the same i.e. the h_1 field completely overlaps with h and H_1 and H_2 are a ortogonal mix of the fields h_2 and h_3.

Through this parametrization we can *a priori* ensure a positively defined set scalar states i.e. no tachyonic states as well as account for unboundness from bellow in our numerical scans.

Likewise, further bellow, in the quark sector, it will also be shown how it is possible to for a set of VEVs determine before hand the tree-level physical masses for quarks and their proper mixing parameters as to respect the CKM matrix. This inversion will also be key as to ensure we have points in our scans that are all in accordance with quark physics.

4.3 Introducing the Yukawa sector

Moving onto the Yukawa portion of the Model, we can write the Yukawa sector to be,

$$\begin{aligned}\mathcal{L}_Y = -\sum_{k=1}^{3}\Big[\overline{Q}_{L_a}\left(\Gamma_k\right)_{ab}\sigma_k n_{R_b} + \overline{Q}_{L_a}\left(\Delta_k\right)_{ab}\tilde{\phi}_k p_{R_b} + h.c.\Big]\\ + \left(\Psi_{L_a}\left(Y_1^e\right)_{ab}\phi_1 e_{R_b} + \text{h.c}\right)\end{aligned} \tag{4.36}$$

Here we see the quark and lepton interactions, note that Γ_k and Δ_k are the down and up Yukawa matrices in the 3HDM model respectively, one for each, k, generation. Notice how the leptons couple only to the first generation Higgs Doublet. This translates into the lepton Yukawa matrix being diagonal as in the SM, allowing leptons to couple exclusively to the lightest doublet, ϕ_1,

$$Y_1^e = \frac{\sqrt{2}}{v_1}M_{\text{diag.}}\left(m_e, m_\mu, m_\tau\right) \tag{4.37}$$

Note that there are no neutrino right handed fields, just like in the SM in Eq. 4.36. Furthermore, examining the effects the imposed symmetry, $\text{U}(1)\times\mathbb{Z}_2$, had on the at the shape of the Yukawa matrices leads us to discover their texture.

$$\begin{aligned}
\Gamma_1 &= \begin{pmatrix}0&0&0\\0&0&0\\\times&\times&0\end{pmatrix}, \quad \Delta_1 = \begin{pmatrix}0&0&0\\0&0&0\\0&0&0\end{pmatrix},\\
\Gamma_2 &= \begin{pmatrix}\times&\times&0\\\times&\times&0\\0&0&0\end{pmatrix}, \quad \Delta_2 = \begin{pmatrix}\times&\times&0\\\times&\times&0\\0&0&0\end{pmatrix},\\
\Gamma_3 &= \begin{pmatrix}0&0&0\\0&0&0\\0&0&\times\end{pmatrix}, \quad \Delta_3 = \begin{pmatrix}0&0&0\\0&0&0\\0&0&\times\end{pmatrix}.
\end{aligned} \tag{4.38}$$

Note, here the $\times$ represent a complex non-zero value in the respective matrix. We can immediately see the treatment of the first generation of quarks differ. These textures of the Yukawa matrices and the size of their components will determine the strength of FCNCs at tree and loop-levels.

The quadratic terms that spawn in the Lagrangian after SBB have the following relations to the Yukawa matrices,

$$\begin{aligned} M_n &= \frac{v_1}{\sqrt{2}}\Gamma_1 + \frac{v_2}{\sqrt{2}}\Gamma_2 + \frac{v_3}{\sqrt{2}}\Gamma_3 \quad , \\ M_p &= \frac{v_1}{\sqrt{2}}\Delta_1 + \frac{v_2}{\sqrt{2}}\Delta_2 + \frac{v_3}{\sqrt{2}}\Delta_3 \quad . \end{aligned} \tag{4.39}$$

Here we begin to see for the first time the origin of the tree-level FCNCs given the Yukawa textures. We observe the following mass terms,

$$M_n = \begin{pmatrix} \times & \times & 0 \\ \times & \times & 0 \\ 0 & 0 & \times \end{pmatrix} \quad M_p = \begin{pmatrix} \times & \times & 0 \\ \times & \times & 0 \\ \times & \times & \times \end{pmatrix} \tag{4.40}$$

Note that there is no overlap between matrix elements inside the up or down sectors, e.g for the case of the $(m_p)_{31}$ and $(m_p)_{32}$ only the first matrix, Γ_1 contributes for it's value,

$$(M_p)_{31} = \frac{1}{\sqrt{2}}v_1(\Gamma_1)_{31} \quad , \quad (M_p)_{32} = \frac{1}{\sqrt{2}}v_1(\Gamma_1)_{32} \tag{4.41}$$

However, we must be able to transform the unphysical n and p into their proper quark fields d and u respectively. This, like in the SM, is achieved by a set of bi-unitarity transformations, $V_{L,R}$ and $U_{L,R}$, that will relate the Gauge basis and the mass basis. Where naturally the CKM matrix will be $V_{\text{CKM}} = V_L^\dagger U_R$. These matrices are defined such,

$$\begin{aligned} m^u_{\text{diag}} &= V_L^n M_n V_R^n \approx V_L^n \begin{pmatrix} \times & \times & 0 \\ \times & \times & 0 \\ 0 & 0 & \times \end{pmatrix} V_R^n \\ m^d_{\text{diag}} &= U_L^p M_p U_R^p \approx U_L^p \begin{pmatrix} \times & \times & 0 \\ \times & \times & 0 \\ \times & \times & \times \end{pmatrix} U_R^p \end{aligned} \tag{4.42}$$

This then imposes certain shapes to the unitary transformations we apply,

$$\begin{aligned} V_L^p = \begin{pmatrix} \times & \times & 0 \\ \times & \times & 0 \\ 0 & 0 & 1 \end{pmatrix} \quad V_R^p &= \begin{pmatrix} \times & \times & 0 \\ \times & \times & 0 \\ 0 & 0 & e^{i\alpha} \end{pmatrix} \\ U_{L,R}^n = \begin{pmatrix} \times & \times & \times \\ \times & \times & \times \\ \times & \times & \times \end{pmatrix} \end{aligned} \tag{4.43}$$

We introduce a complex phase in $V_{L,R}^p$ so that these matrices can be parametrized with two angles. While the parametrization of $U_{L,R}^n$ will require 3. We know these to be the physical degrees of freedom that will be included in the CKM matrix. The CKM matrix elements can then be expressed as,

$$V_{CKM} = V_L^p {U_R^n}^\dagger$$

$$\begin{pmatrix} V_{ud} & V_{us} & V_{ub} \\ V_{cd} & V_{cs} & V_{cb} \\ V_{td} & V_{ts} & V_{tb} \end{pmatrix} = \begin{pmatrix} V_{L,11}^p & V_{L,12}^p & 0 \\ V_{L,21}^p & V_{L,22}^p & 0 \\ 0 & 0 & e^{i\alpha} \end{pmatrix} \begin{pmatrix} U_{R,11}^n & U_{R,12}^n & U_{R,13}^n \\ U_{R,21}^n & U_{R,22}^n & U_{R,23}^n \\ U_{R,31}^n & U_{R,32}^n & U_{R,33}^n \end{pmatrix}^\dagger \tag{4.44}$$

While by moving to the mass basis, where the physical quark mass forms and fields are redefined to include the unitarity transformations. We can write that $U_L^\dagger = V_{\text{CKM}}^\dagger V_L^\dagger$, which together with,

$$\begin{aligned} M_u^{\text{diag}} &= U_L M_p U_R \\ M_d^{\text{diag}} &= V_{\text{CKM}}^\dagger U_L^\dagger M_n U_R \end{aligned} \tag{4.45}$$

allow for a system of coupled linear equations that can be solved with respect to the Yukawa textures and return their values for a given set of Unitary matrices.

4.4 The BGL-like suppression of FCNCs in the 3HDM model

Let us now analyse carefully the Yukawa couplings between the neutral scalar eigenstates and the physical quarks, with particular attention to any FCNC couplings which may arise. Using a new FCNC intermediate basis for the CP-even scalars,

$$\begin{pmatrix} H_0 \\ H_1' \\ H_2' \end{pmatrix} = \mathcal{O}_{\text{FCNC}} \begin{pmatrix} h_1 \\ h_2 \\ h_3 \end{pmatrix} \tag{4.46}$$

where,

$$\mathcal{O}_{\text{FCNC}} = \begin{pmatrix} \frac{v_1}{v} & \frac{v_2}{v} & \frac{v_2}{v} \\ \frac{v_3}{v_{13}} & 0 & \frac{-v_1}{v_{13}} \\ \frac{v_1 v_2}{v v_{13}} & \frac{-v_{13}}{v} & \frac{v_2 v_3}{v v_{13}} \end{pmatrix} \tag{4.47}$$

such that, $v_{13} = \sqrt{v_1^2 + v_3^2}$. Here the state H_0 is exactly the SM Higgs since we are working in the alignment limit, while the states $H_{2,3}'$ are a orthogonal mix of the real states $H_{2,3}$. In terms of quark field interactions with these states in the gauge basis we have,

$$\mathcal{L}_Y^{\text{CP-even}} = -\frac{1}{\sqrt{2}} \left[\overline{n}_L \left(\sum_{k=1}^{3} \Gamma_k h_k \right) n_R + \overline{p}_L \left(\sum_{k=1}^{3} \Delta_k h_k \right) p_R + \text{h.c.} \right] \tag{4.48}$$

This can be represented in terms of the field H_0 as,

$$\mathcal{L}_Y^{H_0} = -\frac{H_0}{v} \left[\overline{n}_L \left(\sum_{k=1}^{3} \Gamma_k v_k \right) n_R + \overline{p}_L \left(\sum_{k=1}^{3} \Delta_k v_k \right) p_R + \text{h.c.} \right] \tag{4.49}$$

Where we can replace the result seen in, 4.39,

$$\mathcal{L}_Y^{H_0} = \frac{H_0}{v} \overline{n}_L M_n n_R + \overline{p}_L M_p p_R \tag{4.50}$$

Showing that the SM like Higgs in our model has the same type of tree-level coupling as in the SM.

Meanwhile for the, generally, heavier states $H_{2,3}'$ we can write their coupling to down quarks as,

$$\mathcal{L}_Y^{H_1', H_2'} = \frac{H_1'}{v} \overline{n}_L N_{d\,1} n_R + \frac{H_2'}{v} \overline{n}_L N_{d\,2} n_R + \text{h.c.} \tag{4.51}$$

where the matrix terms $N_{d\,1}$ and $N_{d\,2}$ can be shown to be,

$$\begin{aligned} N_{d\,1} &= \frac{v}{\sqrt{2} v_{13}} U_L^\dagger \left(\Gamma_1 v_3 - \Gamma_3 v_1 \right) \\ N_{d\,2} &= U_L^\dagger \left[\frac{v_2}{v_{13}} \frac{1}{\sqrt{2}} \left(\gamma_1 v_1 + \gamma_3 v_3 \right) - \frac{v_{13}}{v_2} \frac{1}{\sqrt{2}} \Gamma_2 v_2 \right] U_R \end{aligned} \tag{4.52}$$

To simply the expression of these interaction terms we go back to the textures of the Yukawas, from the block structures presented, and by virtue of our choice to keep the third row of U_L the same as the CKM matrix,

$$(U_L)_{3j} = V_{3j} \tag{4.53}$$

There-for by defining the simple projection operator, P as,

$$P = \begin{pmatrix} 0 & 0 & 0 \\ 0 & 0 & 0 \\ 0 & 0 & 1 \end{pmatrix} \tag{4.54}$$

We can in the down sector Yukawa matrices write,

$$\Gamma_3 = (\Gamma_3)_{33} P \quad , \quad \frac{1}{\sqrt{2}} (\Gamma_1 v_3 - \Gamma_3 v_1) = P M_d \tag{4.55}$$

Hence,

$$\begin{aligned} (N_{d\,1})_{ij} =& \frac{v v_3}{v_1 v_{13}} V_{3i}^* V_{3j} (M_d)_{jj} - \frac{1}{\sqrt{2}} \frac{v v_{13}}{v_1} (\Gamma_3)_{33} V_{3i}^* (U_R)_{3B} \\ (N_{d\,2})_{ij} =& \frac{v_{13}}{v_2} (M_d)_{jj} \delta_{ij} + \left(\frac{v_{13}}{v_2} + \frac{v_2}{v_{13}} \right) V_{3i}^* V_{3j} (M_d)_{jj} \end{aligned} \tag{4.56}$$

We can see trough the proper expansion of these terms that all non diagonal terms, (where $j \neq i$) of $N_{d\,2}$, contain one CKM matrix term. While for $N_{d\,1}$ we have two CKM matrix terms. Even given these terms we must suppress the size of the elements in Γ_1.

A similar procedure in the up quark sector would reveal that there are no scalar mediated FCNCs at tree level in the up sector. This is due to the special structures of the up type Yukawa matrices, we can see Δ_1 is a empty matrix and this prevents FCNCs.

4.5 Numerical Results

4.5.1 Additional Methodology

The methodology used in this numerical analysis is very similar to the introduced in the B-L-SM section. However with two new additions, first the use of the python3 package called `flavio` [93]. The goal of which was to enable our simulations to use the existence of FCNCs to constrict our parameter space. The process of calculations, included the request to SPheno to ensure the calculate all Wilson coefficients. In turn these were fed into `flavio` which calculated predicted FCNC values for our points. We calculated a large number of flavour violating processes in this fashion, in fact, 31 fractions between expected FCNCs in the 3HDM and the expected theoretical value of the SM were calculated. Of these 5 were particularly controlled as they were the only ones that represented significant deviations from the SM values. The second key difference, was the inclusion of a inverted process trough which we ensure the *alignment limit*. Achieved, trough the parametrization of the scalar sector as seen in Eqs, , we not only guarantee sum of VEVs to be approximately 246 GeV, we also ensure the h1 state to be 125.09 GeV for all points. This means the parameters we scanned over with our Monte-Carlo method were the, ψ_1 and ψ_2 VEV parametrization angles, and the scalar couplings λ_{3-10} and the soft breaking term μ_{23}. The scanning limits of which are seen in the Table,

$\psi_{1,2}$; $\beta_{1,2}$; α_3	$\|\mu_{23}\|$	λ_{3-10}
$0 - 2\pi$	1 GeV – 10 TeV	$10^{-7} - 4\pi$

Recall that alignment is only the first phase of our phenomenological scan and a set of equations is solved as to ensure that for each combination of VEVs proper Yukawa couplings are supplied as to reproduce correct quark physics.

Also a important foot-note is unlike the B-L-SM here we only considered tree-level values for calculate observables. This relaxes the difficulty of ensuring the alignment limit and proper quark masses, however radiative and loop corrections could prove to be beneficial to pass certain constraints in our model.

This case was not taken into account in our analysis.

4.5.2 Constraints

As for any BSM theory we must ensure that it cannot be supper-seeded at describing particle interactions by the SM. This, especially for mustiscalar models, requires checking a large numbers of bounds that are imposed on the complex parameter space. Given the large scalar content of the 3HDM special attention needs to be focussed on the possibility of the scalar potential becoming **unbounded-from-below**. Some necessary conditions are easy to find, looking at Eq. 4.4, such as the following couplings being positive so that the potential does not tend towards $-\infty$ when the squared fields become large.

$$\lambda_1 > 0 \quad , \quad \lambda_2 > 0 \quad , \quad \lambda_3 > 0 \quad , \tag{4.57}$$

To further find the proper conditions we must follow a procedure similar to the one used in the 2HDM [79]. By taking two doublets at a time (i, j) to infinity but such that ensuring that $\phi_i^\dagger \phi_j = 0$ (which is easily accomplish-able, if for one doublet the upper components are zero and for the other one the lower components vanish) one obtains a positive value of the potential for any value of the fields if,

$$\lambda_4 > -2\sqrt{\lambda_1\lambda_2} \quad , \quad \lambda_5 > -2\sqrt{\lambda_1\lambda_3} \quad , \quad \lambda_6 > -2\sqrt{\lambda_2\lambda_3} \tag{4.58}$$

We can also adapt the bounded-from-below necessary conditions from ref. [94] (their expressions 21–24), being careful with the fact that the potential of that work is different from ours. This translates into a generalisation of the above conditions, which become

$$\begin{gathered}\lambda_4 > -2\sqrt{\lambda_1\lambda_2} - \min(0, \lambda_7) \quad , \quad \lambda_5 > -2\sqrt{\lambda_1\lambda_3} - \min(0, \lambda_8 - 2\|\lambda_{10}\|) \\ \lambda_6 > -2\sqrt{\lambda_2\lambda_3} - \min(0, \lambda_9) \quad .\end{gathered} \tag{4.59}$$

These conditions eliminate a great deal of parameter space, and though they are not sufficient ones, they should cover most of the parameter space leading to an unbounded-from-below potential.

Other bounds are applied in the potential, such as the **upper perturbatively bound**, ensuring all scalar couplings are maintained bellow 4π.

As to constrain the **unitarity**, one must calculate the scattering amplitudes of scalar to scalar elastic interaction processes. In multiple scalar models a so called S-matrix (S for scattering), comprised of all these amplitudes, has to be diagonalized, checked for unitarity, and ensure that at high energies we respect the "optical theorem". We could adopt a calculation as seen in Ref [94], but given it's complexity we left this calculation for such a large system to SPheno.

Finally, a "standard" constraint on multiscalar models is to verify their compliance with **electroweak** precision bounds or **STU** bounds [95]. We also perform this analysis as in the B-L-SM. Models with N Higgs doublets automatically satisfy $\rho = 1$ at tree-level, meaning bounds on the oblique parameter S will be easily satisfied. These parameters are also calculated by SPheno.

We also studied a wide range of **FCNCs**. Specifically we choose to constraint with the following channels, $B \to \chi_s\gamma$, $B_s \to \mu\mu$, $B_0 \to \mu\mu$, ΔM_s , ΔM_d and $\Delta\varepsilon_K$. Here ΔM_s and ΔM_d represent the frequencies for $B_{0s} - B_{0s}$ and $B_{0d} - B_{0s}$ oscillations respectively. The specific 1 and 2 sigma bounds were achieved by calculating the error rate, E_r,

$$E_r = \frac{\text{Exp}_{BR}}{\text{SM}_{BR}} \times \left(\sqrt{\frac{\text{SM}_{error}}{\text{SM}_{BR}}}\right)^2 + \left(\frac{\text{exp}_{error}}{\text{exp}_{BR}}\right)^2 \tag{4.60}$$

where Exp_{BR} and Exp_{error} stand for the experimentally measured central value at 95% C.L. for a given FCNC and it's experimental error respectively, while the SM_{BR} and SM_{error} stands for the

FCNCs predicted theoretical value for the SM and it's theoretical uncertainty respectively. We can see the values for all given observables at,

Channel	SM_{BR}	SM_{error}	$\exp_{BR}$	$\exp_{error}$
$\mathrm{BR}(B \to \chi_s \gamma)$	0.000329098480234567	1.8753692226475842e-05	3.32e-4	0.16e-4
$\mathrm{BR}(B_s \to \mu\mu)$	3.6677553688451335e-09	1.665939466746625e-10	2.8e-9	0.06e-9
$\mathrm{BR}(B_0 \to \mu\mu)$	1.1426049562685573e-10	1.185537416071237e-11	0.39e-9	0.14e-9
$\mathrm{BR}(\Delta M_s)$	3.9783855435954255e-13	5.0765155526926005e-14	3.334e-13	0.013e-13
$\mathrm{BR}(\Delta M_d)$	1.2498291268113782e-11	7.080484361041182e-13	1.1688e-11	0.0014e-11
$\mathrm{BR}(\Delta \varepsilon_K)$	0.0018127443728339833	0.0002001268596414098	2.228e-3	0.011e-3

why are these the most stringent?

Here we can clearly one of the indicators that the SM might be incomplete, by comparing the $\mathrm{BR}(B_0 \to \mu^-\mu^+)$ values for the SM vs predictions, one is about ,2×10^{-10}, while the SM bound is 1.26×10^{-10}.

4.5.3 Discussion of results

The main objective of our work was to design a tool with whom we can probe large and complicated parameter spaces of BSM models. This was achieved by creating a series of inter connected scripts that create a random scan over a given range.

Here we would like to present the conclusions we can take from a random 3HDM scan with flavour as a chief constricting factor. All flavour observables were kept within the 2 σ limit.

Unitarity, Electroweak and Higgs Sector Cuts

We can begin by observing the available scalar space.

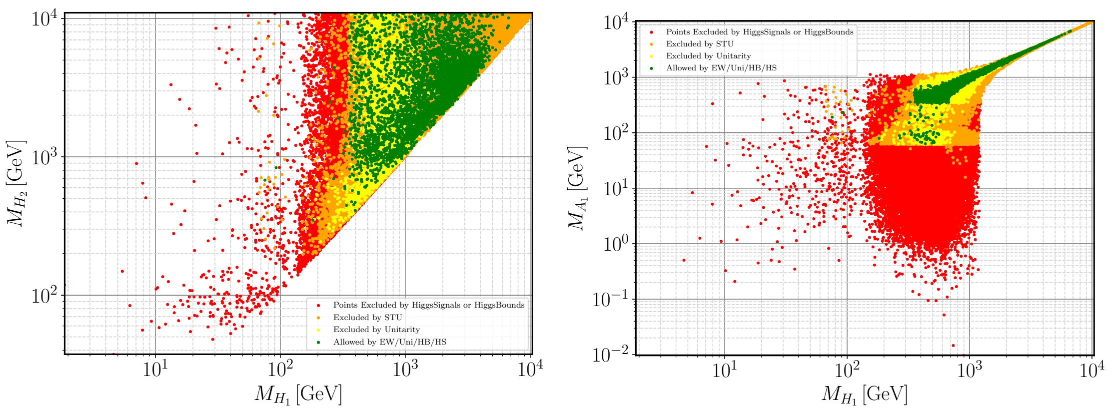

Figure 4.1: Scatter plots of parameter space allowed under several cuts imposed on the BGL-like 3HDM. Right we have the plot showing the masses of the two heavier CP-even scalars H_2 and H_1 while in the right we show the relation between the lightest (non SM Higgs) of the CP-even and pseudoscalar particles. Red points failed HS and HB tests; yellow points violate unitarity constraints; orange points only fail electroweak precision constraints, and green ones satisfy all restrictions.

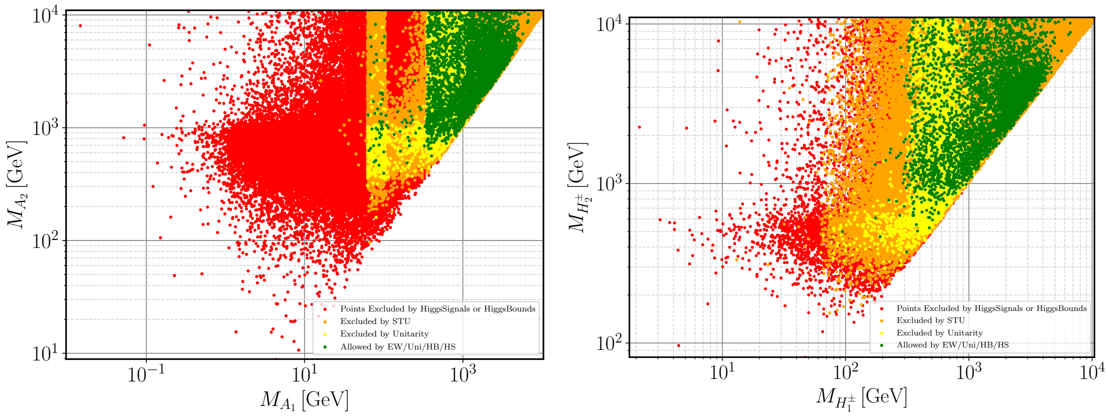

Figure 4.2:

Figure 4.3: Here we can see the remaining CP-odd scalars and how they are excluded under several cuts. Right we have the pseudoscalar masses A_1 and A_2 while in the left side we have the CP- odd charged Higgs states $H_1^\pm$ and $H_2^\pm$. Red points failed HS and HB tests; yellow points violate unitarity constraints; orange points only fail electroweak precision constraints, and green ones satisfy all restrictions.

We can see that there a mass ordering between the scalar states, this is a automatic feature of SPheno that ensures a growing order of scalar masses. This change does not have any real physical significance but it leaves our graphs with a linear cut where $m_i = m_j$. We also omit showing the precise EW ellipsoids seeing their cuts are already shown in these figures. should I show this?

why do pseudo scalar masses tend to funnel?

what can I saw about the bottom graphics

Note that, by requiring that we have a SM-like Higgs boson, naturally imposes conditions upon the couplings of the heavier (or lighter) CP-even scalar states to the Gauge bosons, and seeing that the harshest condition on most scalar sectors is the di-Z production we then have that due to the alignment limit imposed the majority of the scalar sector is allowed.

We can also see that unless the signal coming from the pseudoscalar masses is masked by the Higgs SM signal or the pseudoscalar is heavy (in the TeV region) that it poses a harsh cut on the parameter space.

Why then are the pseudoscalars so constricted.

4.5.4 Flavour results

After being finished with the analysis for the scalar sector we can see exactly what the flavour observables can tell us. We define the exclusion of a point based flavour observables as it being over a 2σ bound for that QFV.

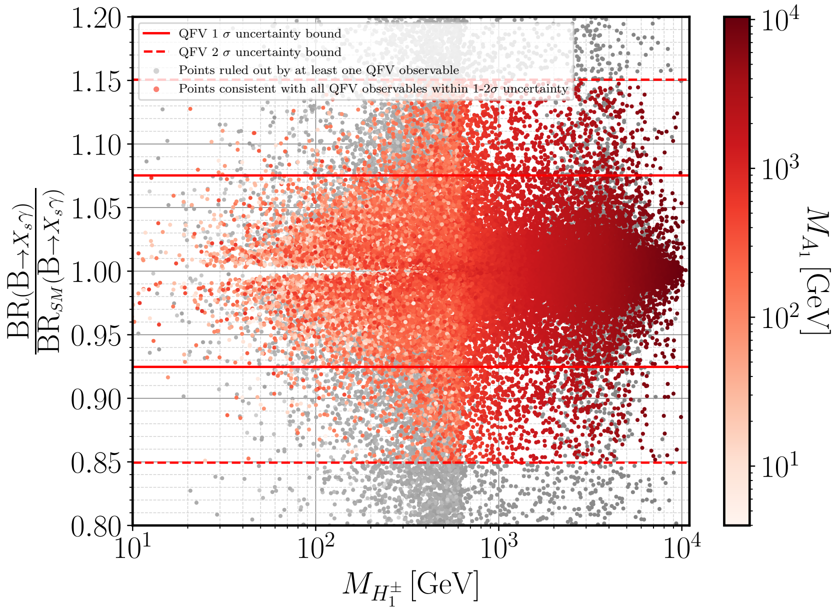

Figure 4.4:

Fine-Tuning

4.5.5 Flavour and Scalar cuts

Having shown that there are no instances of heavy fine tuning in our model.

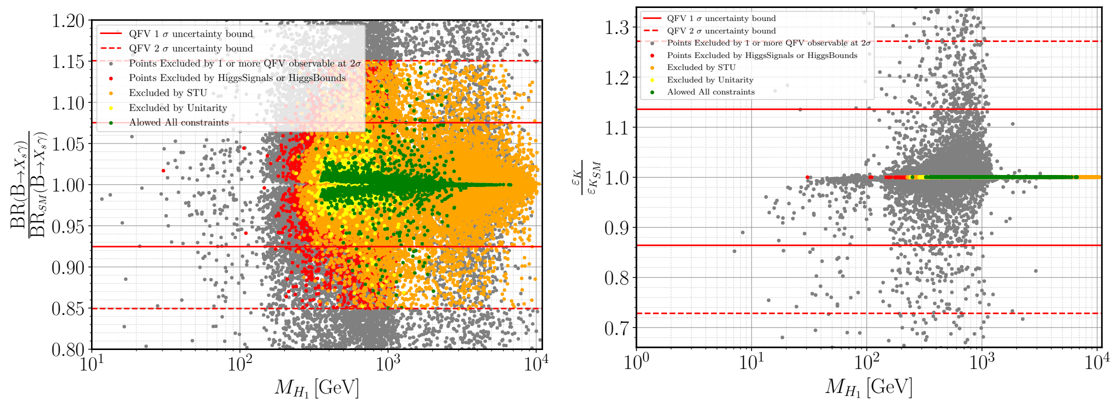

Figure 4.5: Scatter plots of parameter space allowed under several cuts imposed on the BGL-like 3HDM. Right we have the plot showing the masses of the two heavier CP-even scalars H_2 and H_1 while in the right we show the relation between the lightest (non-h) of the CP-even and pseudoscalar particles. Red points failed HS and HB tests; yellow points violate unitarity constraints; orange points only fail electroweak precision constraints, and green ones satisfy all restrictions.

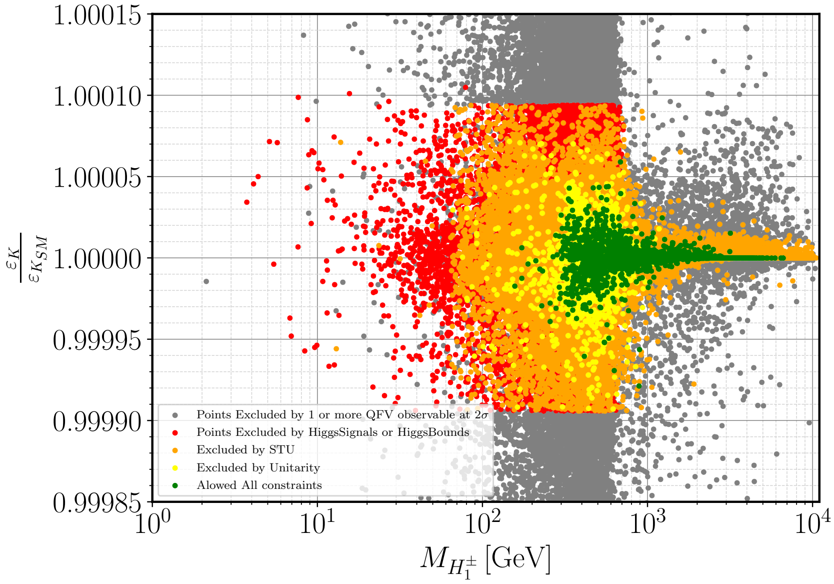

1.00015
1.00010
1.00005
1.00000
0.99995
0.99990
0.99985
$\frac{\varepsilon_K}{\varepsilon_{K_{SM}}}$
10^0
10^1
10^2
10^3
10^4
$M_{H_1^\pm}$ [GeV]
Points Excluded by 1 or more QFV observable at 2σ
Points Excluded by HiggsSignals or HiggsBounds
Excluded by STU
Excluded by Unitarity
Alowed All constraints

Figure 4.6:

Chapter 5

Future Work

Chapter 6

Appendix

6.0.1 Gamma Matrices

The γ matrices are defined as,

$$\{\gamma^\mu, \gamma^\nu\} = 2g^{\mu\nu} I \tag{6.1}$$

where,

$$g^{\mu\nu} = \begin{pmatrix} 1 & 0 & 0 & 0 \\ 0 & -1 & 0 & 0 \\ 0 & 0 & -1 & 0 \\ 0 & 0 & 0 & -1 \end{pmatrix} \tag{6.2}$$

and if $\gamma_\mu = (\gamma^0, \boldsymbol{\gamma})$ then it is usual to require for the hermitian conjugate matrices,

$$\gamma^{0\dagger} = \gamma^0 \quad \text{and} \quad \boldsymbol{\gamma}^\dagger = -\boldsymbol{\gamma} \tag{6.3}$$

6.1 The loop integral $\mathrm{T}_7(x, y, x)$

In Appendix B of Ref. [69], the exact integral equations for $\mathrm{T}_7\,(x, y, z)$ are provided. In our analysis we consider the limit where $x \gg y = z$, with $x = m_{Z'}^2$ and $y = z = m_t^2$, where Eq. (3.43) provides a good approximation up to a truncation error. Here, we show the main steps in determining Eq. (3.43). The exact form of the loop integral reads as

$$\begin{aligned} \mathrm{T}_7\,(x, y, y) = &- \frac{1}{x^2}\varphi_0\,(y, y) + 2y\frac{\partial^3\Phi(x, y, y)}{\partial x \partial y^2} + \frac{\partial^2\Phi(x, y, y)}{\partial x^2} + x\frac{\partial^3\Phi(x, y, y)}{\partial x^2 \partial y} \\ &+ \frac{\Phi(x, y, y)}{x^2} - \frac{1}{x}\frac{\partial\Phi(x, y, y)}{\partial x} + \frac{\partial^2\Phi(x, y, y)}{\partial x \partial y}\,, \end{aligned} \tag{6.4}$$

with $\varphi_0(x, y)$ and $\Phi(x, y, z)$ defined in Ref. [69]. Let us now expand each of the terms for $x \ll y$. While the first term is exact and has the form

$$-\frac{1}{x^2}\varphi_0\,(y, y) = -2\frac{y}{x^2}\log^2 y\,, \tag{6.5}$$

the second can be approximated to

$$2y\frac{\partial^3\Phi(x, y, y)}{\partial x \partial y^2} \simeq \xi\frac{24}{x} = \frac{8}{x} \text{ for } \xi = \frac{1}{3}\,. \tag{6.6}$$

In Eq. (6.6), the $\xi = \frac{1}{3}$ factor was introduced in order to compensate for a truncation error. This was obtained by comparing the numerical values of the exact expression and our approximation. The third term can be simplified to

$$\frac{\partial^2 \Phi(x,y,y)}{\partial x^2} \simeq \frac{2}{x}\left(\log y - \log\frac{y}{x}\right) + \frac{2}{x}\,, \tag{6.7}$$

and the fourth to

$$x\frac{\partial^3 \Phi(x,y,y)}{\partial x^2 \partial y} \simeq -\frac{4}{x}\left(\log\frac{y}{x} + 1\right)\,. \tag{6.8}$$

The fifth and the seventh terms read

$$\frac{\Phi(x,y,y)}{x^2} - \frac{1}{x}\frac{\partial \Phi(x,y,y)}{\partial x} \simeq \frac{2}{x}\log\frac{1}{x}\,, \tag{6.9}$$

and finally, the sixth terms can be expanded as

$$\frac{\partial^2 \Phi(x,y,y)}{\partial x \partial y} \simeq \frac{4}{x}\left(\log\frac{y}{x} - 1\right)\,. \tag{6.10}$$

Noting that Eq. (6.5) is of the order $\frac{1}{x^2}$, putting together Eqs. (6.4), (6.6), (6.7), (6.8), (6.9), and (6.10) we get for the leading $\frac{1}{x}$ contributions the following:

$$\mathrm{T}_7\,(x,y,y) \simeq \overbrace{\frac{2}{x}\left(\log y - \log\frac{y}{x}\right) + \frac{2}{x}\log\frac{1}{x}}^{0} \overbrace{-\frac{4}{x}\left(\log\frac{y}{x} + 1\right) + \frac{4}{x}\left(\log\frac{y}{x} - 1\right)}^{-\frac{8}{x}} + \frac{8}{x} + \frac{2}{x} \simeq \frac{2}{x}\,. \tag{6.11}$$

Bibliography

[1] G. Aad, T. Abajyan, B. Abbott, J. Abdallah, S. Abdel Khalek, A. Abdelalim, O. Abdinov, R. Aben, B. Abi, M. Abolins, and et al., "Observation of a new particle in the search for the standard model higgs boson with the atlas detector at the lhc," *Physics Letters B*, vol. 716, p. 1–29, Sep 2012.

[2] S. Chatrchyan, V. Khachatryan, A. M. Sirunyan, A. Tumasyan, W. Adam, E. Aguilo, T. Bergauer, M. Dragicevic, J. Er, C. Fabjan, *et al.*, "Observation of a new boson at a mass of 125 gev with the cms experiment at the lhc," *Physics Letters B*, vol. 716, no. 1, pp. 30–61, 2012.

[3] C. Collaborations *et al.*, "Combined measurement of the higgs boson mass in pp collisions at sqrt s = 7 and 8 tev with the atlas and cms experiments," *arXiv preprint arXiv:1503.07589*, 2015.

[4] C. Collaborations *et al.*, "Measurements of the higgs boson production and decay rates and constraints on its couplings from a combined atlas and cms analysis of the lhc pp collision data at sqrt s = 7 and 8 tev," *arXiv preprint arXiv:1606.02266*, 2016.

[5] L. Bergström, "Non-baryonic dark matter: observational evidence and detection methods," *Reports on Progress in Physics*, vol. 63, p. 793–841, Apr 2000.

[6] U. Sarkar, *Particle and Astroparticle Physics*, vol. 1 of *1*. The name of the publisher, 1 ed., 12 2007.

[7] D. E. Morrissey and M. J. Ramsey-Musolf, "Electroweak baryogenesis," *New Journal of Physics*, vol. 14, p. 125003, Dec. 2012.

[8] F. Capozzi, E. Lisi, and A. Marrone, "Neutrino mass hierarchy and electron neutrino oscillation parameters with one hundred thousand reactor events," *Phys. Rev. D*, vol. 89, p. 013001, Jan 2014.

[9] M. Ilyushin, P. Mandrik, and S. Slabospitskii, "Constraints on the higgs boson anomalous fcnc interactions with light quarks," *Nuclear Physics B*, vol. 952, p. 114921, 2020.

[10] K. Huitu and N. Koivunen, "Suppression of scalar mediated FCNCs in a SU(3)c× SU(3)l× u(1)x -model," *Journal of High Energy Physics*, vol. 2019, Oct. 2019.

[11] A. Salam and J. Ward, "Electromagnetic and weak interactions," *Physics Letters*, vol. 13, no. 2, pp. 168 – 171, 1964.

[12] M. W. Grünewald, "6 experimental precision tests for the electroweak standard model," *Landolt-Börnstein - Group I Elementary Particles, Nuclei and Atoms*, p. 166–224, 2008.

[13] N. Foundation, "The nobel prize in physics," 1979.

[14] E. Noether, "Invariant variation problems," *Transport Theory and Statistical Physics*, vol. 1, no. 3, pp. 186–207, 1971.

[15] P. W. Higgs, "Broken symmetries and the masses of gauge bosons," *Physical Review Letters*, vol. 13, no. 16, p. 508, 1964.

[16] F. Englert and R. Brout, "Broken symmetry and the mass of gauge vector mesons," *Physical Review Letters*, vol. 13, no. 9, p. 321, 1964.

[17] G. Guralnik, C. Hagen, and T. Kibble, "Global conservation laws and massless particles 1964 phys," *Rev. Lett*, vol. 13, no. 585, p. 169, 1964.

[18] H. D. Politzer, "Reliable perturbative results for strong interactions?," *Physical Review Letters*, vol. 30, no. 26, p. 1346, 1973.

[19] D. J. Gross and F. Wilczek, "Ultraviolet behavior of non-abelian gauge theories," *Physical Review Letters*, vol. 30, no. 26, p. 1343, 1973.

[20] C. Quigg, *GAUGE THEORIES OF THE STRONG, WEAK AND ELECTROMAGNETIC INTERACTIONS*, vol. 56. 1983.

[21] J. H. Christenson, J. W. Cronin, V. L. Fitch, and R. Turlay, "Evidence for the 2π decay of the k_2^0 meson," *Phys. Rev. Lett.*, vol. 13, pp. 138–140, Jul 1964.

[22] N. Foundation, "The nobel prize in physics," 1979.

[23] M. Tanabashi, K. Hagiwara, K. Hikasa, K. Nakamura, Y. Sumino, F. Takahashi, J. Tanaka, K. Agashe, G. Aielli, C. Amsler, M. Antonelli, D. Asner, H. Baer, S. Banerjee, R. Barnett, T. Basaglia, C. Bauer, J. Beatty, V. Belousov, J. Beringer, S. Bethke, A. Bettini, H. Bichsel, O. Biebel, K. Black, E. Blucher, O. Buchmuller, V. Burkert, M. Bychkov, R. Cahn, M. Carena, A. Ceccucci, A. Cerri, D. Chakraborty, M.-C. Chen, R. Chivukula, G. Cowan, O. Dahl, G. D'Ambrosio, T. Damour, D. de Florian, A. de Gouvêa, T. DeGrand, P. de Jong, G. Dissertori, B. Dobrescu, M. D'Onofrio, M. Doser, M. Drees, H. Dreiner, D. Dwyer, P. Eerola, S. Eidelman, J. Ellis, J. Erler, V. Ezhela, W. Fetscher, B. Fields, R. Firestone, B. Foster, A. Freitas, H. Gallagher, L. Garren, H.-J. Gerber, G. Gerbier, T. Gershon, Y. Gershtein, T. Gherghetta, A. Godizov, M. Goodman, C. Grab, A. Gritsan, C. Grojean, D. Groom, M. Grünewald, A. Gurtu, T. Gutsche, H. Haber, C. Hanhart, S. Hashimoto, Y. Hayato, K. Hayes, A. Hebecker, S. Heinemeyer, B. Heltsley, J. Hernández-Rey, J. Hisano, A. Höcker, J. Holder, A. Holtkamp, T. Hyodo, K. Irwin, K. Johnson, M. Kado, M. Karliner, U. Katz, S. Klein, E. Klempt, R. Kowalewski, F. Krauss, M. Kreps, B. Krusche, Y. Kuyanov, Y. Kwon, O. Lahav, J. Laiho, J. Lesgourgues, A. Liddle, Z. Ligeti, C.-J. Lin, C. Lippmann, T. Liss, L. Littenberg, K. Lugovsky, S. Lugovsky, A. Lusiani, Y. Makida, F. Maltoni, T. Mannel, A. Manohar, W. Marciano, A. Martin, A. Masoni, J. Matthews, U.-G. Meißner, D. Milstead, R. Mitchell, K. Mönig, P. Molaro, F. Moortgat, M. Moskovic, H. Murayama, M. Narain, P. Nason, S. Navas, M. Neubert, P. Nevski, Y. Nir, K. Olive, S. P. Griso, J. Parsons, C. Patrignani, J. Peacock, M. Pennington, S. Petcov, V. Petrov, E. Pianori, A. Piepke, A. Pomarol, A. Quadt, J. Rademacker, G. Raffelt, B. Ratcliff, P. Richardson, A. Ringwald, S. Roesler, S. Rolli, A. Romaniouk, L. Rosenberg, J. Rosner, G. Rybka, R. Ryutin, C. Sachrajda, Y. Sakai, G. Salam, S. Sarkar, F. Sauli, O. Schneider, K. Scholberg, A. Schwartz, D. Scott, V. Sharma, S. Sharpe, T. Shutt, M. Silari, T. Sjöstrand, P. Skands, T. Skwarnicki, J. Smith, G. Smoot, S. Spanier, H. Spieler, C. Spiering, A. Stahl, S. Stone, T. Sumiyoshi, M. Syphers, K. Terashi, J. Terning, U. Thoma, R. Thorne, L. Tiator, M. Titov, N. Tkachenko, N. Törnqvist, D. Tovey, G. Valencia, R. V. de Water, N. Varelas, G. Venanzoni, L. Verde, M. Vincter, P. Vogel, A. Vogt, S. Wakely, W. Walkowiak, C. Walter, D. Wands, D. Ward, M. Wascko, G. Weiglein, D. Weinberg, E. Weinberg, M. White, L. Wiencke, S. Willocq, C. Wohl, J. Womersley, C. Woody, R. Workman, W.-M. Yao, G. Zeller, O. Zenin, R.-Y. Zhu, S.-L. Zhu, F. Zimmermann, P. Zyla, J. Anderson, L. Fuller, V. Lugovsky, and P. S. and, "Review of particle physics," *Physical Review D*, vol. 98, Aug. 2018.

[24] S. L. Glashow, J. Iliopoulos, and L. Maiani, "Weak interactions with lepton-hadron symmetry," *Physical review D*, vol. 2, no. 7, p. 1285, 1970.

[25] E. G. and, "Flavour anomalies: a review," *Journal of Physics: Conference Series*, vol. 1137, p. 012025, Jan. 2019.

[26] S. Fajfer, J. F. Kamenik, and I. Nišandžić, "B→ $d * \tau\nu\tau$ sensitivity to new physics," *Physical Review D*, vol. 85, May 2012.

[27] R. N. Mohapatra and R. E. Marshak, "Local B-L Symmetry of Electroweak Interactions, Majorana Neutrinos and Neutron Oscillations," *Phys. Rev. Lett.*, vol. 44, pp. 1316–1319, 1980. [Erratum: Phys. Rev. Lett.44,1643(1980)].

[28] L. Basso, S. Moretti, and G. M. Pruna, "Constraining the g_1' coupling in the minimal $B - L$ Model," *J. Phys.*, vol. G39, p. 025004, 2012.

[29] L. Basso, S. Moretti, and G. M. Pruna, "Theoretical constraints on the couplings of non-exotic minimal Z' bosons," *JHEP*, vol. 08, p. 122, 2011.

[30] M. Tanabashi *et al.*, "Review of Particle Physics," *Phys. Rev.*, vol. D98, no. 3, p. 030001, 2018.

[31] G. Degrassi, S. Di Vita, J. Elias-Miro, J. R. Espinosa, G. F. Giudice, G. Isidori, and A. Strumia, "Higgs mass and vacuum stability in the Standard Model at NNLO," *JHEP*, vol. 08, p. 098, 2012.

[32] S. Alekhin, A. Djouadi, and S. Moch, "The top quark and Higgs boson masses and the stability of the electroweak vacuum," *Phys. Lett.*, vol. B716, pp. 214–219, 2012.

[33] D. Buttazzo, G. Degrassi, P. P. Giardino, G. F. Giudice, F. Sala, A. Salvio, and A. Strumia, "Investigating the near-criticality of the Higgs boson," *JHEP*, vol. 12, p. 089, 2013.

[34] M. S. Chanowitz, J. R. Ellis, and M. K. Gaillard, "The Price of Natural Flavor Conservation in Neutral Weak Interactions," *Nucl. Phys.*, vol. B128, pp. 506–536, 1977.

[35] H. Fritzsch and P. Minkowski, "Unified Interactions of Leptons and Hadrons," *Annals Phys.*, vol. 93, pp. 193–266, 1975.

[36] H. Georgi and D. V. Nanopoulos, "T Quark Mass in a Superunified Theory," *Phys. Lett.*, vol. 82B, pp. 392–394, 1979.

[37] H. Georgi and D. V. Nanopoulos, "Ordinary Predictions from Grand Principles: T Quark Mass in O(10)," *Nucl. Phys.*, vol. B155, pp. 52–74, 1979.

[38] H. Georgi and D. V. Nanopoulos, "Masses and Mixing in Unified Theories," *Nucl. Phys.*, vol. B159, pp. 16–28, 1979.

[39] Y. Achiman and B. Stech, "Quark Lepton Symmetry and Mass Scales in an E6 Unified Gauge Model," *Phys. Lett.*, vol. 77B, pp. 389–393, 1978.

[40] F. Gursey, P. Ramond, and P. Sikivie, "A Universal Gauge Theory Model Based on E6," *Phys. Lett.*, vol. 60B, pp. 177–180, 1976.

[41] F. Gursey and M. Serdaroglu, "E6 GAUGE FIELD THEORY MODEL REVISITED," *Nuovo Cim.*, vol. A65, p. 337, 1981. [,271(1981)].

[42] V. Barger, P. Langacker, M. McCaskey, M. Ramsey-Musolf, and G. Shaughnessy, "Complex Singlet Extension of the Standard Model," *Phys. Rev.*, vol. D79, p. 015018, 2009.

[43] T. Yanagida, "Horizontal gauge symmetry and masses of neutrinos," *Conf. Proc.*, vol. C7902131, pp. 95–99, 1979.

[44] M. Gell-Mann, P. Ramond, and R. Slansky, "Complex Spinors and Unified Theories," *Conf. Proc.*, vol. C790927, pp. 315–321, 1979.

[45] R. N. Mohapatra and G. Senjanovic, "Neutrino Mass and Spontaneous Parity Nonconservation," *Phys. Rev. Lett.*, vol. 44, p. 912, 1980. [,231(1979)].

[46] K. Kaneta, Z. Kang, and H.-S. Lee, "Right-handed neutrino dark matter under the $B-L$ gauge interaction," *JHEP*, vol. 02, p. 031, 2017.

[47] N. Okada and O. Seto, "Higgs portal dark matter in the minimal gauged $U(1)_{B-L}$ model," *Phys. Rev.*, vol. D82, p. 023507, 2010.

[48] S. Okada, "Z' Portal Dark Matter in the Minimal $B-L$ Model," *Adv. High Energy Phys.*, vol. 2018, p. 5340935, 2018.

[49] M. Fukugita and T. Yanagida, "Baryogenesis Without Grand Unification," *Phys. Lett.*, vol. B174, pp. 45–47, 1986.

[50] A. Pilaftsis, "CP violation and baryogenesis due to heavy Majorana neutrinos," *Phys. Rev.*, vol. D56, pp. 5431–5451, 1997.

[51] A. Pilaftsis and T. E. J. Underwood, "Resonant leptogenesis," *Nucl. Phys.*, vol. B692, pp. 303–345, 2004.

[52] S. Khalil, "TeV-scale gauged B-L symmetry with inverse seesaw mechanism," *Phys. Rev.*, vol. D82, p. 077702, 2010.

[53] F. F. Deppisch, S. Kulkarni, and W. Liu, "Searching for a light $Z\prime$ through Higgs production at the LHC," *Phys. Rev.*, vol. D100, no. 11, p. 115023, 2019.

[54] M. Aaboud *et al.*, "Search for new high-mass phenomena in the dilepton final state using 36 fb^{-1} of proton-proton collision data at $\sqrt{s} = 13$ TeV with the ATLAS detector," *JHEP*, vol. 10, p. 182, 2017.

[55] A. Czarnecki and W. J. Marciano, "The Muon anomalous magnetic moment: A Harbinger for 'new physics'," *Phys. Rev.*, vol. D64, p. 013014, 2001.

[56] S. Khalil and C. S. Un, "Muon Anomalous Magnetic Moment in SUSY B-L Model with Inverse Seesaw," *Phys. Lett.*, vol. B763, pp. 164–168, 2016.

[57] J.-L. Yang, T.-F. Feng, Y.-L. Yan, W. Li, S.-M. Zhao, and H.-B. Zhang, "Lepton-flavor violation and two loop electroweak corrections to $(g-2)_\mu$ in the B-L symmetric SSM," *Phys. Rev.*, vol. D99, no. 1, p. 015002, 2019.

[58] W. Porod, "SPheno, a program for calculating supersymmetric spectra, SUSY particle decays and SUSY particle production at e+ e- colliders," *Comput. Phys. Commun.*, vol. 153, pp. 275–315, 2003.

[59] W. Porod and F. Staub, "SPheno 3.1: Extensions including flavour, CP-phases and models beyond the MSSM," *Comput. Phys. Commun.*, vol. 183, pp. 2458–2469, 2012.

[60] F. Staub, "SARAH," 2008.

[61] F. Staub, "SARAH 4 : A tool for (not only SUSY) model builders," *Comput. Phys. Commun.*, vol. 185, pp. 1773–1790, 2014.

[62] P. Bechtle, O. Brein, S. Heinemeyer, O. Stål, T. Stefaniak, G. Weiglein, and K. E. Williams, "HiggsBounds − 4: Improved Tests of Extended Higgs Sectors against Exclusion Bounds from LEP, the Tevatron and the LHC," *Eur. Phys. J.*, vol. C74, no. 3, p. 2693, 2014.

[63] P. Bechtle, S. Heinemeyer, O. Stål, T. Stefaniak, and G. Weiglein, "*HiggsSignals*: Confronting arbitrary Higgs sectors with measurements at the Tevatron and the LHC," *Eur. Phys. J.*, vol. C74, no. 2, p. 2711, 2014.

[64] J. Alwall, R. Frederix, S. Frixione, V. Hirschi, F. Maltoni, O. Mattelaer, H. S. Shao, T. Stelzer, P. Torrielli, and M. Zaro, "The automated computation of tree-level and next-to-leading order differential cross sections, and their matching to parton shower simulations," *JHEP*, vol. 07, p. 079, 2014.

[65] R. Costa, A. P. Morais, M. O. P. Sampaio, and R. Santos, "Two-loop stability of a complex singlet extended Standard Model," *Phys. Rev.*, vol. D92, p. 025024, 2015.

[66] A. Freitas, J. Lykken, S. Kell, and S. Westhoff, "Testing the Muon g-2 Anomaly at the LHC," *JHEP*, vol. 05, p. 145, 2014. [Erratum: JHEP09,155(2014)].

[67] S. M. Barr and A. Zee, "Electric Dipole Moment of the Electron and of the Neutron," *Phys. Rev. Lett.*, vol. 65, pp. 21–24, 1990. [Erratum: Phys. Rev. Lett.65,2920(1990)].

[68] V. Ilisie, "New Barr-Zee contributions to $(\mathbf{g-2})$- in two-Higgs-doublet models," *JHEP*, vol. 04, p. 077, 2015.

[69] T.-F. Feng and X.-Y. Yang, "Renormalization and two loop electroweak corrections to lepton anomalous dipole moments in the standard model and beyond (I): Heavy fermion contributions," *Nucl. Phys.*, vol. B814, pp. 101–141, 2009.

[70] S. Weinberg, "Gauge theory ofCPNonconservation," *Physical Review Letters*, vol. 37, pp. 657–661, Sept. 1976.

[71] T. D. Lee, "A theory of SpontaneousTViolation," *Physical Review D*, vol. 8, pp. 1226–1239, Aug. 1973.

[72] G. C. Branco, L. Lavoura, and J. P. Silva, *CP Violation*, vol. 103. 1999.

[73] P. Ferreira, L. Lavoura, and J. P. Silva, "A soft origin for ckm-type cp violation," *Physics Letters B*, vol. 704, p. 179–188, Oct 2011.

[74] M. Nebot and J. P. Silva, "Self-cancellation of a scalar in neutral meson mixing and implications for the lhc," *Physical Review D*, vol. 92, Oct 2015.

[75] P. M. Ferreira and L. Lavoura, "No strong *cp* violation up to the one-loop level in a two-higgs-doublet model," 2019.

[76] A. Pich and P. Tuzón, "Yukawa alignment in the two-higgs-doublet model," *Physical Review D*, vol. 80, Nov 2009.

[77] M. Jung, A. Pich, and P. Tuzón, "Charged-higgs phenomenology in the aligned two-higgs-doublet model," *Journal of High Energy Physics*, vol. 2010, Nov 2010.

[78] M. Jung, A. Pich, and P. Tuzón, "$b^- \to \chi s \gamma$ rate and cp asymmetry within the aligned two-higgs-doublet model," *Physical Review D*, vol. 83, Apr 2011.

[79] G. Branco, W. Grimus, and L. Lavoura, "Relating the scalar flavour-changing neutral couplings to the ckm matrix," *Physics Letters B*, vol. 380, p. 119–126, Jul 1996.

[80] L. LAVOURA, "MODELS OF CP VIOLATION EXCLUSIVELY VIA NEUTRAL-SCALAR EXCHANGE," *International Journal of Modern Physics A*, vol. 09, pp. 1873–1888, Apr. 1994.

[81] F. J. Botella, G. C. Branco, A. Carmona, M. Nebot, L. Pedro, and M. N. Rebelo, "Physical constraints on a class of two-higgs doublet models with fcnc at tree level," *Journal of High Energy Physics*, vol. 2014, Jul 2014.